

Performance Limits of Single-Anchor Millimeter-Wave Positioning

Anastasios Kakkavas, *Student Member, IEEE*, Mario H. Castañeda Garcia,
Richard A. Stirling-Gallacher, and Josef A. Nassek, *Life Fellow, IEEE*

Abstract

The fundamental limits of single-anchor multi-antenna positioning are investigated. Exploiting the structure of the multiple input-multiple output-orthogonal frequency division multiplexing (MIMO-OFDM) channel at millimeter-wave frequencies, we present geometrically intuitive asymptotic expressions for the Fisher information on position, orientation and velocity for large bandwidth and number of antennas. The effects of synchronization errors and mobility are studied and it is shown that non-line-of-sight (NLOS) paths can be used to estimate the synchronization error and drastically improve the positioning performance. We also find that, in the presence of line-of-sight (LOS), mobility has a small impact on the achievable positioning accuracy, but in the NLOS-only scenario it can significantly improve the achievable performance, depending on the variance of the synchronization error. Finally, considering a communication system with device-specific transmission and reception constraints, we compare the positioning accuracy between the downlink and the uplink and show that they are equivalent under the same signal-to-noise ratio (SNR).

Index Terms

mm-Wave, single-anchor positioning, TDOA, TOA, AOD AOA, synchronization, Doppler shift, Fisher information, Cramér-Rao lower bound, downlink, uplink

A. Kakkavas, M. H. Castañeda Garcia and R. A. Stirling-Gallacher are with the Munich Research Center, Huawei Technologies Duesseldorf GmbH, 80992 Munich, Germany (e-mail: {anastasios.kakkavas, mario.castaneda, richard.sg}@huawei.com). A. Kakkavas and J. A. Nassek are with the Department of Electrical and Computer Engineering, Technical University of Munich, 80333 Munich, Germany (e-mail: josef.a.nassek@tum.de). J. A. Nassek is also with the Department of Teleinformatics Engineering, Federal University of Ceara, 60020-180 Fortaleza, Brazil

I. INTRODUCTION

The 5th generation (5G) of wireless communication networks is on its way, with the vision of providing unprecedentedly high data rates, massive connectivity and reduced latency, among others, which can be enabled by the large bandwidth available at millimeter-wave (mm-Wave) frequencies, massive number of antennas and dense deployment of base stations. Coincidentally or not, these enablers provide fertile ground for a radical improvement of the positioning capabilities of wireless communication networks [1] and bring localization to the foreground of 5G development. Apart from fusion with Global Navigation Satellite Systems (GNSS) to enhance traditional positioning services, the expected improvement of localization accuracy of communication networks can be a key driving force in the realization of scenarios such as assisted living [2], smart factories [3] and automated driving [4], [5], where GNSS and other existing technologies may not be able to guarantee the desired positioning accuracy under all conditions. Moreover, it is anticipated that position information will be used as an input to communication-related tasks, such as proactive resource allocation [6], beamforming [7] and beam-alignment [8].

In an effort to unlock the great potential of next generation wireless communication networks, numerous works on the topic have been published. Theoretical analyses for positioning under a multi-anchor setup have been presented in [9]–[13]. Despite promising high accuracy, multi-anchor positioning might be impossible at mm-Wave due to the lack of significantly strong links to two or more anchors. In mm-Wave frequencies the path loss between isotropic antennas¹ is increased as a consequence of their decreased effective area/aperture and beamforming gains are required to compensate for it. On the other hand, the fact that more antennas can be packed in the same physical area allows for multi-antenna transceivers, which enable accurate angle of departure (AOD) and angle of arrival (AOA) estimation. Also, the large bandwidth available at mm-Wave frequencies enables accurate time of arrival (TOA) or time difference of arrival (TDOA) measurements. Hence, reliable position estimation is possible with a single anchor.

In recent years, many studies on single-anchor positioning have been published. The single-anchor localization bounds were derived in [14] for arrays with different beamforming strategies, under line-of-sight (LOS)-only propagation, taking synchronization errors and beamforming

¹Isotropic antennas are only assumed as a theoretical tool; in practice, antenna elements with potentially similar, but not identical, properties are used.

weights' quantization errors into account. This work was extended in [15] including MIMO transmission and multipath propagation. In [16] the Cramér-Rao lower bound (CRLB) for single-anchor LOS positioning was presented, deriving a necessary condition on the reference signal for a non-singular Fisher information matrix (FIM). The authors of [17] provided asymptotic expressions for the position error bounds in sparse mm-Wave channels with large bandwidth and large number of antennas, and conducted a comparison between downlink and uplink positioning. In [18] it was shown that the FIM provided by single-bounce NLOS paths is rank-1 and analytic expressions for the direction and intensity of position and orientation information were obtained. In [19], the single-anchor localization error bounds with a multicarrier waveform were derived and an algorithm approaching these bounds for a high SNR was presented. Considering general non-orthogonal waveforms and TOA and AOA-based positioning, the authors of [20] showed analytically that multipath effects vanish in the large array regime and developed a novel bound-achieving direct localization algorithm. Single-anchor positioning algorithms have also been presented in [21] and [22]. Apart from [14] and [15], the aforementioned works assume no synchronization errors, which is difficult to obtain in practical communication systems. To address this issue, the authors of [23] propose a two-way localization protocol. In [24] a joint localization and synchronization algorithm is presented for a network with a single anchor and multiple full-duplex agents.

Following previous works [17]–[19], we study the performance limits of two-dimensional (2D) single-anchor multi-antenna positioning in sparse mm-Wave channels, where only single-bounce NLOS paths are assumed strong enough for reception [25]–[28]. We extend prior works by considering three aspects: a multicarrier waveform², the impact of synchronization errors and mobility. To this end, we provide an analysis of the Fisher information associated with position, orientation, and velocity estimation in mm-Wave MIMO systems. The main contributions of this work are the following:

- When both the transmitter (Tx) and receiver (Rx) are static (static scenario), we show that the directions of information provided by the single-bounce NLOS paths depend only on the geometry of the channel and not on the system parameters.
- When the receiver or the transmitter is moving (dynamic scenario), we study the effect of

²The results are also applicable for the single-carrier frequency division multiple access (SC-FDMA) with appropriate design of the reference signal.

the Doppler shift on the Fisher information. We prove that the information provided by each single-bounce NLOS path is rank-2.

- For the static and dynamic scenario, the impact of the synchronization error is analytically investigated and numerical evaluations of its effect on positioning with or without the LOS path are provided.
- We compare downlink (DL) and uplink (UL) positioning under device-specific Tx/Rx constraints and show that the link with the highest receive SNR offers the highest accuracy. For perfectly synchronized and asynchronous systems we show that the FIMs of the position and orientation parameters in the DL and the UL differ only by a scalar, which is equal to the ratio of the receive SNR in the DL and the UL.

The rest of the paper is organized as follows. The system model is derived in Section II. In Section III, the Cramér-Rao bound for position and orientation estimation in the static and dynamic scenario is derived. The relation between DL and UL positioning is derived in Section IV. The asymptotic analysis and geometric interpretation of the Fisher information are provided in Section V. Numerical evaluations of the bounds are provided in Section VI. Section VII concludes the work.

Notation: We use bold lowercase for column vectors, bold uppercase for matrices, non-bold for scalars and calligraphic letters for sets. Depending on its argument, $|\cdot|$ denotes the absolute value of a scalar, the determinant of a matrix or the cardinality of a set. The operators $(\cdot)^T$ and $(\cdot)^H$ denote the transpose and the conjugate transpose of a vector or matrix, $\|\cdot\|_2$ denotes the Euclidean norm of a vector and $\Re\{\cdot\}$ and $\Im\{\cdot\}$ denote the real and imaginary part of a complex number. The i -th element of a vector and the (i, j) -th element of a matrix are denoted by $[\cdot]_i$ and $[\cdot]_{i,j}$, respectively. The expectation operator is denoted by $\mathbb{E}[\cdot]$ and the sets of real and complex numbers are denoted by \mathbb{R} and \mathbb{C} . A multivariate circularly symmetric complex Gaussian distribution with mean $\boldsymbol{\mu}$ and covariance matrix \boldsymbol{C} is denoted by $\mathcal{N}_{\mathbb{C}}(\boldsymbol{\mu}, \boldsymbol{C})$. A list of frequently used symbols is provided in Table I.

II. SYSTEM MODEL

In this section we present the signal model when both the transmitter and the receiver are static, and then we extend the model to the dynamic scenario, where either the transmitter or the receiver is moving.

TABLE I
LIST OF FREQUENTLY USED SYMBOLS

$\mathbf{p}_T, \alpha_T, \mathbf{v}_T$	Tx position, orientation and velocity	$t_{\text{rms},l}$	root mean square duration of the signal propagated through path l
$\mathbf{p}_R, \alpha_R, \mathbf{v}_R$	Rx position, orientation and velocity	ρ_l	transverse velocity component of path l
$\mathbf{p}_{s,l}$	position of l -th scatterer/reflector	N, \mathcal{P}, N_B	number of subcarriers, set of used subcarriers and number of OFDM symbols
$d_{T,R}$	Tx-Rx distance	F_s, f_c, c	sampling rate, carrier frequency and speed of light
$d_{T,s,l}, d_{R,s,l}$	distance of the l -th scatterer/reflector from the Tx and the Rx	P_T, γ_p	Tx power and its fraction allocated to sub-carrier p
$\mathbf{u}(\theta), \mathbf{u}_\perp(\theta)$	unit vectors at angles θ and $\theta - \pi/2$	β	effective baseband bandwidth
N_T, M_T	number of Tx antennas and beamforming vectors	$\bar{\omega}_c$	effective carrier angular frequency
N_R, M_R	number of Rx antennas and beamforming vectors	$\epsilon_{\text{clk}}, \sigma_{\text{clk}}^2$	clock synchronization error and its variance
$S_T(\tilde{\theta}), S_R(\tilde{\theta})$	Tx and Rx squared array aperture function	$\sigma_{\eta,R}^2$	noise variance per dimension
L	number of propagation paths	$\delta_{R,T}$	receive SNR
$\tau_l, \theta_{T,l}, \theta_{R,l}, h_l$	TOA, AOD, AOA and gain of path l		
ξ_i	intensity effect of Doppler shift on path l		

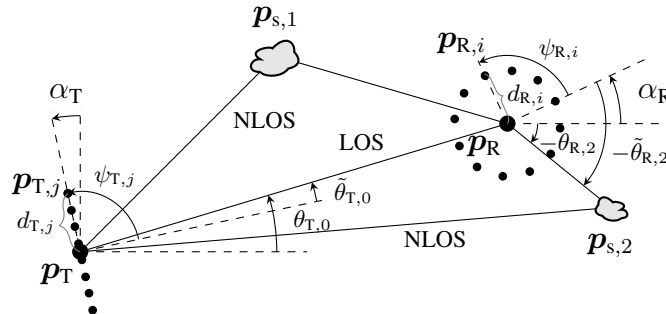


Fig. 1. Geometric model, example with a uniform linear array (ULA) at the transmitter and a uniform circular array (UCA) at the receiver.

A. Static Scenario

1) *Geometry*: In Fig. 1 an example of the considered 2D setup is shown. The Tx and Rx have N_T and N_R antennas with reference points $\mathbf{p}_T = [p_{T,x}, p_{T,y}]^T \in \mathbb{R}^2$ and $\mathbf{p}_R = [p_{R,x}, p_{R,y}]^T \in \mathbb{R}^2$. Their orientation with respect to (w.r.t.) the horizontal line is α_T and α_R , respectively. The position of the j -th element of the Tx array is

$$\mathbf{p}_{T,j} = \mathbf{p}_T + d_{T,j} \mathbf{u}(\psi_{T,j} + \alpha_T) = [p_{T,j,x}, p_{T,j,y}]^T \in \mathbb{R}^2, \quad j = 1, \dots, N_T, \quad (1)$$

where $\mathbf{u}(\psi) = [\cos(\psi), \sin(\psi)]^T$ and $d_{T,j}$ and $\psi_{T,j} + \alpha_T$ are its distance and angle from the Tx reference point, as shown in Fig. 1. The quantities for the Rx array are defined accordingly.

We assume that for all the antenna pairs there are L discrete propagation paths. The first path ($l = 0$) is either the LOS path, if it exists, or a single-bounce NLOS path, while the rest $L - 1$ are single-bounce NLOS paths ($l = 1, \dots, L - 1$). The point of incidence of the l -th single-bounce path, which corresponds either to scattering or reflection, is $\mathbf{p}_{s,l} = [p_{s,l,x}, p_{s,l,y}]^T$. The array apertures are assumed to be small compared to the distance between Tx and Rx, as well as the distance between each of the scatterers/reflectors and the transmitter and receiver. Therefore, the delay of path l from Tx element j to Rx element i can be approximated by $\tau_{l,i,j} \approx \tau_l - \tau_{T,j}(\tilde{\theta}_{T,l}) - \tau_{R,i}(\tilde{\theta}_{R,l})$, $l = 0, \dots, L - 1$, where

$$\tau_l = \begin{cases} \|\mathbf{p}_R - \mathbf{p}_T\|_2 / c, & \text{if the } l\text{-th path is LOS,} \\ (\|\mathbf{p}_{s,l} - \mathbf{p}_T\|_2 + \|\mathbf{p}_R - \mathbf{p}_{s,l}\|_2) / c, & \text{otherwise,} \end{cases} \quad (2)$$

$\tau_{T,j}(\tilde{\theta}_{T,l}) = d_{T,j} \mathbf{u}^T(\psi_{T,j}) \mathbf{u}(\tilde{\theta}_{T,l}) / c$, and $\tau_{R,i}(\tilde{\theta}_{R,l}) = d_{R,i} \mathbf{u}^T(\psi_{R,i}) \mathbf{u}(\tilde{\theta}_{R,l}) / c$, with c being the speed of light. We assume without loss of generality that $\tau_0 \leq \tau_1 \leq \dots \leq \tau_{L-1}$. The angles are defined as $\tilde{\theta}_{T,l} = \theta_{T,l} - \alpha_T$, $\tilde{\theta}_{R,l} = \theta_{R,l} - \alpha_R$, $l = 0, \dots, L - 1$, where $\theta_{T,0} = \text{atan2}(p_{R,y} - p_{T,y}, p_{R,x} - p_{T,x})$, $\theta_{R,0} = \theta_{T,0} + \pi$, $\theta_{T,l} = \text{atan2}(p_{s,l,y} - p_{T,y}, p_{s,l,x} - p_{T,x}) - \alpha_T$ and $\theta_{R,l} = \text{atan2}(p_{s,l,y} - p_{R,y}, p_{s,l,x} - p_{R,x}) - \alpha_R$, $l = 1, \dots, L - 1$, with $\text{atan2}(y, x)$ being the four-quadrant inverse tangent function.

2) *Signal Model*: Assuming high resolution analog-to-digital conversion (ADC) and digital-to-analog conversion (DAC), such that the system is practically linear, the pulse $\tilde{g}(t)$ models all the Tx and Rx processing steps, namely upsampling, digital Tx filtering/pulse shaping, DAC, analog Tx and Rx filtering, ADC, digital Rx filtering/pulse shaping and downsampling. Hence, the discrete-time channel impulse response between Tx antenna j and Rx antenna i is

$$c_{i,j}[m] = \sum_{l=0}^{L-1} h'_l \tilde{g}(mT_s - \tau_{l,i,j}) e^{-j2\pi f_c \tau_{l,i,j}}, \quad (3)$$

where T_s is the sampling period, $F_s = 1/T_s$ is the sampling rate and $h'_l \in \mathbb{C}$, $l = 0, \dots, L - 1$, are the gains of the propagation paths. Then, the received signal at antenna i for sample n is

$$[\tilde{\mathbf{r}}[n]]_i = \sum_{j=1}^{N_T} \sum_{m=-\infty}^{\infty} c_{i,j}[m] [\tilde{\mathbf{x}}[n - m]]_j + [\tilde{\boldsymbol{\eta}}[n]]_i, \quad (4)$$

where $\tilde{\mathbf{x}}[n] \in \mathbb{C}^{N_T}$ is the time-domain transmit signal at sample n and $\tilde{\boldsymbol{\eta}}[n]$ is the zero-mean circularly-symmetric Gaussian noise vector, which is temporally and spatially uncorrelated with variance $2\sigma_{\eta,R}^2$ per-antenna, i.e. $\tilde{\boldsymbol{\eta}}[n] \sim \mathcal{N}_{\mathbb{C}}(\mathbf{0}, 2\sigma_{\eta,R}^2 \mathbf{I}_{N_R})$.

We consider a Cyclic Prefix-OFDM (CP-OFDM) system with N subcarriers and the CP consisting of N_{CP} samples. N_{B} OFDM symbols are transmitted and \mathcal{P} is the set of indices of the loaded subcarriers. In order to ensure there is no inter-symbol interference, the CP is assumed to be long enough to accommodate the effective delay spread of the channel, including the length of the pulse $\tilde{g}(t)$ and the frame synchronization error. In mm-Wave systems the dimensionality of the digital transmit and receive signals may be reduced by hardware constraints, i.e. the transmitter and the receiver may be equipped with $M_{\text{T}} \leq N_{\text{T}}$ and $M_{\text{R}} \leq N_{\text{R}}$ radio frequency (RF) chains, respectively. Therefore, we consider a transmit precoder $\mathbf{F}_{\text{T}} \in \mathbb{C}^{N_{\text{T}} \times M_{\text{T}}}$ and a receive combiner $\mathbf{F}_{\text{R}} \in \mathbb{C}^{N_{\text{R}} \times M_{\text{R}}}$ that are common to all subcarriers. When no precoding (receive combining) is applied $N_{\text{T}} = M_{\text{T}}$ ($N_{\text{R}} = M_{\text{R}}$) and $\mathbf{F}_{\text{T}} = \mathbf{I}_{N_{\text{T}}}$ ($\mathbf{F}_{\text{R}} = \mathbf{I}_{N_{\text{R}}}$). The Tx signal vector at subcarrier p , $p \in \mathcal{P}$, of symbol b , $b = 0, \dots, N_{\text{B}} - 1$, before precoding is $\mathbf{s}_b[p] \in \mathbb{C}^{M_{\text{T}}}$, and after precoding is $\mathbf{x}_b[p] = \mathbf{F}_{\text{T}}^* \mathbf{s}_b[p]$. Without loss of generality, we assume that the reference signal transmission starts at time 0. The time-domain transmit signal (after precoding) $\tilde{\mathbf{x}}[n]$ is related to the b -th time-domain OFDM symbol $\tilde{\mathbf{x}}_b[m]$ as $\tilde{\mathbf{x}}[bM + m] = \tilde{\mathbf{x}}_b[m]$, where $M = N + N_{\text{CP}}$ and $\tilde{\mathbf{x}}_b[m] = \sum_{p \in \mathcal{P}} \mathbf{x}_b[p] e^{j \frac{2\pi}{N} p(m - N_{\text{CP}})} / \sqrt{N}$, $m = 0, \dots, M - 1$.

We assume that the receiver is imperfectly synchronized, it namely works under the premise that the signal was transmitted at ϵ_{clk} , where ϵ_{clk} is the clock synchronization error, which we assume to be a zero-mean Gaussian distributed random variable with variance σ_{clk}^2 . We note that $\sigma_{\text{clk}}^2 = 0$ corresponds to perfectly synchronized clocks and $\sigma_{\text{clk}}^2 \rightarrow \infty$ corresponds to asynchronous operation. After receive combining and Discrete Fourier Transform (DFT), the receiver uses its knowledge of the time of transmission to apply an appropriate per-subcarrier rotation to the post-DFT signal. It can be shown that the resulting signal vector at subcarrier p of symbol b is

$$\mathbf{w}_b[p] \approx \mathbf{F}_{\text{R}}^{\text{H}} \mathbf{H}[p] \mathbf{F}_{\text{T}}^* \mathbf{s}_b[p] + \mathbf{F}_{\text{R}}^{\text{H}} \boldsymbol{\eta}_b[p], \quad (5)$$

where

$$\mathbf{H}[p] = g[p] e^{-j \omega_p \epsilon_{\text{clk}}} \sum_{l=0}^{L-1} h_l e^{-j \omega_p \tau_l} \mathbf{a}_{\text{R},p}(\tilde{\theta}_{\text{R},l}) \mathbf{a}_{\text{T},p}^{\text{T}}(\tilde{\theta}_{\text{T},l}) \in \mathbb{C}^{N_{\text{R}} \times N_{\text{T}}}, \quad (6)$$

$$\mathbf{a}_{\text{T},p}(\tilde{\theta}_{\text{T},l}) = \left[e^{j(\omega_c + \omega_p) \tau_{\text{T},1}(\tilde{\theta}_{\text{T},l)}, \dots, e^{j(\omega_c + \omega_p) \tau_{\text{T},N_{\text{T}}}(\tilde{\theta}_{\text{T},l)} \right]^{\text{T}} \in \mathbb{C}^{N_{\text{T}}}, \quad (7)$$

with $h_l = h'_l e^{-j 2\pi f_c \tau_l}$, $\omega_p = 2\pi p F_s / N$, $\omega_c = 2\pi f_c$ and $\boldsymbol{\eta}_b[p] \sim \mathcal{N}_{\mathbb{C}}(\mathbf{0}, 2\sigma_{\eta,\text{R}}^2 \mathbf{I}_{N_{\text{R}}})$. $\mathbf{a}_{\text{R},p}(\tilde{\theta}_{\text{R},l})$ is defined similarly to $\mathbf{a}_{\text{T},p}(\tilde{\theta}_{\text{T},l})$. We assume that the range of the angles passed as arguments to the array steering vectors is such that, for a given array structure, there is 1-1 mapping between

angles and steering vectors. The approximate equality in (5) follows from the assumption that, apart from being time-limited, $\tilde{g}(t)$ is essentially band-limited.

B. Dynamic Scenario

We now extend the signal model to the dynamic scenario, with the receiver moving with constant velocity $\mathbf{v}_R = [v_{R,x}, v_{R,y}]^T \in \mathbb{R}^2$. Let $n_0 T_s$ be the TOA of the first sample of the received signal fed to the DFT and $\mathbf{p}_{R,0}$ be the receiver's position at that time instant. The position of the receiver at time $n T_s$ is $\mathbf{p}_R(n T_s) = \mathbf{p}_{R,0} + \mathbf{v}_R \cdot (n - n_0) T_s$. As in the static scenario, we make use of the far field assumption, so that the angles and the channel gains are approximately invariant during the observation interval $N_B M T_s$. The received signal at antenna i is

$$[\tilde{\mathbf{r}}[n]]_i = \sum_{j=1}^{N_T} \sum_{m=-\infty}^{\infty} c_{i,j}[m, n] [\tilde{\mathbf{x}}[n - m]]_j + [\tilde{\boldsymbol{\eta}}[n]]_i, \quad (8)$$

where

$$c_{i,j}[m, n] = \sum_{l=0}^{L-1} h'_l \tilde{g}(m T_s - \tau_{l,i,j} + v_l (n - n_0) T_s / c) e^{-j 2\pi f_c (\tau_{l,i,j} - v_l (n - n_0) T_s / c)}, \quad (9)$$

with $v_l = \mathbf{v}_R^T \mathbf{u}(\theta_{R,l})$ being the speed of the receiver in the direction of the AOA. We can show that the signal vector at subcarrier p of symbol b after receive combining is

$$\mathbf{w}_b[p] \approx \sum_{q \in \mathcal{P}} \mathbf{F}_R^H \mathbf{H}_b[p, q] \mathbf{F}_T^* \mathbf{s}_b[q] + \mathbf{F}_R^H \boldsymbol{\eta}_b[p], \quad (10)$$

where

$$\begin{aligned} \mathbf{H}_b[p, q] &= g[q] e^{-j \omega_q \epsilon_{\text{clk}}} \sum_{l=0}^{L-1} h_l e^{-j (\omega_q \tau_l - \frac{\omega_c + \omega_q}{c} v_l b M T_s)} Q \left(\left(\omega_p - \omega_q - \frac{\omega_c + \omega_q}{c} v_l \right) \frac{T_s}{2} \right) \times \\ &\mathbf{a}_{R,q}(\tilde{\theta}_{R,l}) \mathbf{a}_{T,q}^T(\tilde{\theta}_{T,l}) \in \mathbb{C}^{N_R \times N_T}, \end{aligned} \quad (11)$$

with $Q(x) = e^{-j(N-1)x} \sin(Nx) / (N \sin(x))$. The Doppler shift $v_l (\omega_c + \omega_q) / c$ is subcarrier-dependent and an increasing function of the subcarrier index. Similar to [13], we assume that the observation interval is much smaller than the channel coherence time $T_{\text{co}} \propto c / (f_c \|\mathbf{v}_R\|_2)$ [29]. When the transmitter is moving with velocity \mathbf{v}_R and the receiver is static, the signal model (10) is still valid with $v_l = \mathbf{v}_T^T \mathbf{u}(\theta_{T,l})$.

III. COMPUTATION OF THE CRAMÉR-RAO LOWER BOUND

A. Static Scenario

Based on the received signal model (5), we now derive the Fisher information matrix and the Cramér-Rao lower bound for position and orientation estimation for a single-anchor MIMO-OFDM system. Setting $h_{l,\mathfrak{R}} = \Re\{h_l\}$ and $h_{l,\mathfrak{S}} = \Im\{h_l\}$, $l = 0, \dots, L-1$, we define the channel parameter vector ϕ as

$$\phi = [\epsilon_{\text{clk}}, \tau_0, \tilde{\theta}_{\text{T},0}, \tilde{\theta}_{\text{R},0}, h_{0,\mathfrak{R}}, h_{0,\mathfrak{S}}, \dots, \tau_{L-1}, \tilde{\theta}_{\text{T},L-1}, \tilde{\theta}_{\text{R},L-1}, h_{L-1,\mathfrak{R}}, h_{L-1,\mathfrak{S}}]^{\text{T}} \in \mathbb{R}^{5L+1}. \quad (12)$$

The covariance matrix $\mathbf{C}_{\hat{\phi}}$ of any unbiased estimator $\hat{\phi}$ satisfies [30] $\mathbf{C}_{\hat{\phi}} - \mathbf{J}_{\phi}^{-1} \succeq \mathbf{0}$, where $\succeq \mathbf{0}$ denotes positive semi-definiteness and $\mathbf{J}_{\phi} \in \mathbb{R}^{(5L+1) \times (5L+1)}$ is the hybrid FIM of ϕ . \mathbf{J}_{ϕ} is defined as

$$\mathbf{J}_{\phi} = \mathbf{J}_{\phi}^{(\text{p})} + \mathbf{J}_{\phi}^{(\text{o})}, \quad (13)$$

where $\mathbf{J}_{\phi}^{(\text{p})}$ accounts for the prior information on ϕ and $\mathbf{J}_{\phi}^{(\text{o})}$ accounts for the observation-related FI. With ϵ_{clk} being the only parameter with prior information, it is straightforward to find that the only non-zero entry of $\mathbf{J}_{\phi}^{(\text{p})}$ is

$$\left[\mathbf{J}_{\phi}^{(\text{p})}\right]_{1,1} = \mathbb{E} \left[-\frac{\partial^2 \ln p(\epsilon_{\text{clk}})}{\partial \epsilon_{\text{clk}}^2} \right] = \frac{1}{\sigma_{\text{clk}}^2}, \quad (14)$$

where $p(\epsilon_{\text{clk}})$ is the probability density function (pdf) of ϵ_{clk} . Since ϕ is observed under Gaussian noise, the (i, j) -th entry of the $\mathbf{J}_{\phi}^{(\text{o})}$ is

$$\left[\mathbf{J}_{\phi}^{(\text{o})}\right]_{i,j} = \frac{1}{\sigma_{\eta,\text{R}}^2} \sum_{b=1}^{N_{\text{B}}} \sum_{p \in \mathcal{P}} \Re \left\{ \frac{\partial \mathbf{m}_b^{\text{H}}[p]}{\partial \phi_i} (\mathbf{F}_{\text{R}}^{\text{H}} \mathbf{F}_{\text{R}})^{-1} \frac{\partial \mathbf{m}_b[p]}{\partial \phi_j} \right\}, \quad (15)$$

where

$$\mathbf{m}_b[p] = g[p] e^{-j\omega_p \tau_s} \mathbf{F}_{\text{R}}^{\text{H}} \mathbf{H}[p] \mathbf{F}_{\text{T}}^* \mathbf{s}_b[p]. \quad (16)$$

The required derivatives of $\mathbf{m}_b[p]$ are provided in Appendix A.

Instead of ϕ , which includes the unknown channel parameters, we are rather interested in the estimation of a parameter vector including the unknown position parameters. We consider two cases, depending on the available knowledge on the Tx and Rx position and orientation. In the first case, the Tx position \mathbf{p}_{T} and orientation α_{T} are known and the Rx position \mathbf{p}_{R} and orientation α_{R} are unknown (receiver localization). The position parameter vector then reads as

$$\tilde{\phi}_{\text{R}} = \begin{cases} [\mathbf{p}_{\text{R}}^{\text{T}}, \alpha_{\text{R}}, \epsilon_{\text{clk}}, h_{0,\mathfrak{R}}, h_{0,\mathfrak{S}}, \dots, \mathbf{p}_{\text{s},L-1}^{\text{T}}, h_{L-1,\mathfrak{R}}, h_{L-1,\mathfrak{S}}]^{\text{T}} \in \mathbb{R}^{4L+2}, & \text{if LOS exists,} \\ [\mathbf{p}_{\text{R}}^{\text{T}}, \alpha_{\text{R}}, \epsilon_{\text{clk}}, \mathbf{p}_{\text{s},0}, h_{0,\mathfrak{R}}, h_{0,\mathfrak{S}}, \dots, \mathbf{p}_{\text{s},L-1}^{\text{T}}, h_{L-1,\mathfrak{R}}, h_{L-1,\mathfrak{S}}]^{\text{T}} \in \mathbb{R}^{4L+4}, & \text{otherwise.} \end{cases} \quad (17)$$

In the second case, the Rx estimates the Tx position and orientation, knowing its own position and orientation (transmitter localization). The parameter vector is then

$$\tilde{\phi}_T = \begin{cases} [\mathbf{p}_T^T, \alpha_T, \epsilon_{\text{clk}}, h_{0,\mathfrak{R}}, h_{0,\mathfrak{S}}, \dots, \mathbf{p}_{s,L-1}^T, h_{L-1,\mathfrak{R}}, h_{L-1,\mathfrak{S}}]^T \in \mathbb{R}^{4L+2}, & \text{if LOS exists,} \\ [\mathbf{p}_T^T, \alpha_T, \epsilon_{\text{clk}}, \mathbf{p}_{s,0}, h_{0,\mathfrak{R}}, h_{0,\mathfrak{S}}, \dots, \mathbf{p}_{s,L-1}^T, h_{L-1,\mathfrak{R}}, h_{L-1,\mathfrak{S}}]^T \in \mathbb{R}^{4L+4}, & \text{otherwise.} \end{cases} \quad (18)$$

The FIMs $\mathbf{J}_{\tilde{\phi}_R}, \mathbf{J}_{\tilde{\phi}_T}$ can be obtained using \mathbf{J}_ϕ and the transformation matrices $\mathbf{T}_R, \mathbf{T}_T$ [31]:

$$\mathbf{J}_{\tilde{\phi}_R} = \mathbf{T}_R \mathbf{J}_\phi \mathbf{T}_R^T, \quad (19)$$

$$\mathbf{J}_{\tilde{\phi}_T} = \mathbf{T}_T \mathbf{J}_\phi \mathbf{T}_T^T, \quad (20)$$

where $[\mathbf{T}_R]_{i,j} = \partial[\phi]_j / \partial[\tilde{\phi}_R]_i$ and $[\mathbf{T}_T]_{i,j} = \partial[\phi]_j / \partial[\tilde{\phi}_T]_i$. The entries of $\mathbf{T}_R, \mathbf{T}_T$ are given in Appendix B. In the following, we will refer to both $\mathbf{J}_{\tilde{\phi}_R}$ and $\mathbf{J}_{\tilde{\phi}_T}$ as $\mathbf{J}_{\tilde{\phi}}$ and to \mathbf{T}_R and \mathbf{T}_T as \mathbf{T} , explicitly distinguishing between them where necessary.

We use the notion of the equivalent FIM (EFIM) [11] to focus on the available information on the position and orientation parameters. The EFIM can have much lower dimensions than $\mathbf{J}_{\tilde{\phi}}$, but still fully describes the available information on the parameters of interest. Splitting \mathbf{T} as $\mathbf{T} = [\mathbf{T}_{\text{po}}^T, \mathbf{T}_{\text{np}}^T]^T$, with \mathbf{T}_{po} consisting of the first three rows of \mathbf{T} , which correspond to the position and orientation parameters, and \mathbf{T}_{np} containing the rest, the EFIM for the position and orientation parameters is

$$\mathbf{J}_{\text{po}} = \mathbf{T}_{\text{po}} \mathbf{J}_\phi \mathbf{T}_{\text{po}}^T - \mathbf{T}_{\text{po}} \mathbf{J}_\phi \mathbf{T}_{\text{np}}^T (\mathbf{T}_{\text{np}} \mathbf{J}_\phi \mathbf{T}_{\text{np}}^T)^{-1} \mathbf{T}_{\text{np}} \mathbf{J}_\phi \mathbf{T}_{\text{po}}^T. \quad (21)$$

The measure we use for characterizing the achievable position estimation accuracy is the position error bound (PEB) defined as [16]

$$\text{PEB} = \sqrt{[\mathbf{J}_{\text{po}}^{-1}]_{1,1} + [\mathbf{J}_{\text{po}}^{-1}]_{2,2}}. \quad (22)$$

B. Dynamic Scenario

In the dynamic scenario the channel parameter vector ϕ is extended from (12) to

$$\phi = [\epsilon_{\text{clk}}, \tau_0, \tilde{\theta}_{T,0}, \tilde{\theta}_{R,0}, v_0, h_{0,\mathfrak{R}}, h_{0,\mathfrak{S}}, \dots, \tau_{L-1}, \tilde{\theta}_{T,L-1}, \tilde{\theta}_{R,L-1}, v_{L-1}, h_{L-1,\mathfrak{R}}, h_{L-1,\mathfrak{S}}]^T \in \mathbb{R}^{6L+1}. \quad (23)$$

For receiver localization, the position parameter vector is defined as

$$\tilde{\phi}_R = \begin{cases} [\mathbf{p}_R^T, \alpha_R, \mathbf{v}_R, \epsilon_{\text{clk}}, h_{0,\mathfrak{R}}, h_{0,\mathfrak{S}}, \dots, \mathbf{p}_{s,L-1}^T, h_{L-1,\mathfrak{R}}, h_{L-1,\mathfrak{S}}]^T \in \mathbb{R}^{4L+4}, & \text{if LOS exists,} \\ [\mathbf{p}_R^T, \alpha_R, \mathbf{v}_R, \epsilon_{\text{clk}}, \mathbf{p}_{s,0}, h_{0,\mathfrak{R}}, h_{0,\mathfrak{S}}, \dots, \mathbf{p}_{s,L-1}^T, h_{L-1,\mathfrak{R}}, h_{L-1,\mathfrak{S}}]^T \in \mathbb{R}^{4L+6}, & \text{otherwise.} \end{cases} \quad (24)$$

For transmitter localization the position parameter vector can be defined accordingly. We are interested in the EFIM \mathbf{J}_{pov} of the position, orientation and velocity parameters:

$$\mathbf{J}_{\text{pov}} = \mathbf{T}_{\text{pov}} \mathbf{J}_{\phi} \mathbf{T}_{\text{pov}}^{\text{T}} - \mathbf{T}_{\text{pov}} \mathbf{J}_{\phi} \mathbf{T}_{\text{np}}^{\text{T}} (\mathbf{T}_{\text{np}} \mathbf{J}_{\phi} \mathbf{T}_{\text{np}}^{\text{T}})^{-1} \mathbf{T}_{\text{np}} \mathbf{J}_{\phi} \mathbf{T}_{\text{pov}}^{\text{T}}, \quad (25)$$

where we have split \mathbf{T} as $\mathbf{T} = [\mathbf{T}_{\text{pov}}^{\text{T}}, \mathbf{T}_{\text{np}}^{\text{T}}]^{\text{T}}$, with \mathbf{T}_{pov} consisting of the first 5 rows of \mathbf{T} .

IV. DOWNLINK VS UPLINK POSITIONING

In the following, we discuss the positioning and orientation estimation of a user equipment (UE) in a communication system, assuming the position and orientation of the base station (BS) are known. In contrast to [17], we assume that the devices (BS or UE) use the same set of beamforming vectors for transmission and reception, e.g. \mathbf{F}_{R} in the DL is equal to \mathbf{F}_{T} in the UL. We consider this setup because the presence of \mathbf{F}_{T} and \mathbf{F}_{R} usually results from some hardware constraints, which are device-specific and independent of whether the device is in Tx or Rx mode. For example, due to the limited number of RF chains, a UE might only be able to process a signal in Tx and Rx mode with a set of analog beamforming vectors. We consider here the static scenario, but a similar analysis can be conducted in the dynamic scenario. With known BS position and orientation, positioning of a UE in the DL corresponds to receiver localization, whereas positioning of a UE in the UL corresponds to transmitter localization. Thus, by replacing the subscripts 'T' and 'R' with 'BS' and 'UE' in (5) and (6) for the DL and vice-versa for the UL, we obtain the signal model for the DL and the UL, respectively:

$$\text{(DL)} : \quad \mathbf{w}_b^{(\text{DL})}[p] \approx \mathbf{F}_{\text{UE}}^{\text{H}} \mathbf{H}^{(\text{DL})}[p] \mathbf{F}_{\text{BS}}^* \mathbf{s}_b^{(\text{DL})}[p] + \mathbf{F}_{\text{UE}}^{\text{H}} \boldsymbol{\eta}_b[p] \quad (26)$$

$$\text{(UL)} : \quad \mathbf{w}_b^{(\text{UL})}[p] \approx \mathbf{F}_{\text{BS}}^{\text{H}} \mathbf{H}^{(\text{UL})}[p] \mathbf{F}_{\text{UE}}^* \mathbf{s}_b^{(\text{UL})}[p] + \mathbf{F}_{\text{BS}}^{\text{H}} \boldsymbol{\eta}_b[p], \quad (27)$$

where we have that $\mathbf{H}^{(\text{UL})}[p] = (\mathbf{H}^{(\text{DL})}[p])^{\text{T}}$ and that the BS and UE use the same beamforming vectors for transmission and reception, as mentioned above. From the parameter vector for receiver localization (17) and the corresponding parameter vector for transmitter localization (18), it is straightforward to verify that $\tilde{\boldsymbol{\phi}}^{(\text{DL})} = \tilde{\boldsymbol{\phi}}^{(\text{UL})}$.

We now compare the positioning accuracy between the DL and the UL, under the following assumptions:

- 1) \mathbf{F}_{UE} and \mathbf{F}_{BS} have orthonormal columns.
- 2) The signals transmitted through different beamforming vectors are uncorrelated and have equal power, i.e. $\mathbb{E} \left[\mathbf{s}_b^{(\text{DL})}[p] (\mathbf{s}_b^{(\text{DL})}[p])^{\text{H}} \right] = \gamma_p P_{\text{BS}} / M_{\text{BS}}$ and $\mathbb{E} \left[\mathbf{s}_b^{(\text{UL})}[p] (\mathbf{s}_b^{(\text{UL})}[p])^{\text{H}} \right] =$

$\gamma_p P_{\text{UE}}/M_{\text{UE}}$, where γ_p is the fraction of the power of the OFDM symbol that is spent on the p -th subcarrier, with $\sum_{p \in \mathcal{P}} \gamma_p = 1$.

$\mathbf{J}_{\tilde{\phi}}$ in the DL and the UL can be obtained in a similar fashion as \mathbf{J}_{ϕ} in (13), (14) and (15). We define \mathbf{Z} as the matrix which has the same dimensions as $\mathbf{J}_{\tilde{\phi}}$ and its (i, j) -th element is

$$[\mathbf{Z}]_{i,j} = \text{tr} \left(\Re \left\{ \sum_{b=1}^{N_B} \sum_{p \in \mathcal{P}} \mathbf{F}_{\text{BS}}^T \frac{\partial (\mathbf{H}^{(\text{DL})}[p])^H}{\partial \tilde{\phi}_i} \mathbf{F}_{\text{UE}} \mathbf{F}_{\text{UE}}^H \frac{\partial \mathbf{H}^{(\text{DL})}[p]}{\partial \tilde{\phi}_j} \mathbf{F}_{\text{BS}}^* \right\} \right). \quad (28)$$

From (13), (14), (15), (26) and taking the expectation over $\mathbf{s}_b^{(\text{DL})}[p]$ we can compute $\mathbf{J}_{\tilde{\phi}}^{(\text{DL})}$ as

$$\mathbf{J}_{\tilde{\phi}}^{(\text{DL})} = \frac{P_{\text{BS}}}{\sigma_{\eta, \text{UE}}^2 M_{\text{BS}}} \mathbf{Z} + \mathbf{e}_4 \mathbf{e}_4^T \frac{1}{\sigma_{\text{clk}}^2}, \quad (29)$$

where $\sigma_{\eta, \text{UE}}^2$ is the noise variance at the UE in the DL and \mathbf{e}_i is the vector whose i -th entry is equal to 1 and the rest of its entries are 0. Given that $\mathbf{H}_{b,p}^{(\text{UL})} = (\mathbf{H}_{b,p}^{(\text{DL})})^T$ we can show by using simple properties of the trace operator that

$$\mathbf{J}_{\tilde{\phi}}^{(\text{UL})} = \frac{P_{\text{UE}}}{\sigma_{\eta, \text{BS}}^2 M_{\text{UE}}} \mathbf{Z} + \mathbf{e}_4 \mathbf{e}_4^T \frac{1}{\sigma_{\text{clk}}^2}, \quad (30)$$

where $\sigma_{\eta, \text{BS}}^2$ is the noise variance at the BS in the UL. Using the Sherman-Morrison formula we invert $\mathbf{J}_{\tilde{\phi}}^{(\text{DL})}$ and $\mathbf{J}_{\tilde{\phi}}^{(\text{UL})}$ and after a few steps we find that the ratio of the DL and UL PEB (see (22)) is given by

$$\frac{\text{PEB}^{(\text{DL})}}{\text{PEB}^{(\text{UL})}} = \sqrt{\frac{\delta_{\text{UL}} \zeta - \frac{1}{\delta_{\text{DL}} \sigma_{\text{clk}}^2 + [\mathbf{Z}^{-1}]_{4,4}}}{\delta_{\text{DL}} \zeta - \frac{1}{\delta_{\text{UL}} \sigma_{\text{clk}}^2 + [\mathbf{Z}^{-1}]_{4,4}}}}, \quad (31)$$

where $\zeta = ([\mathbf{Z}^{-1}]_{1,1} + [\mathbf{Z}^{-1}]_{2,2}) / (([\mathbf{Z}^{-1}]_{1,4})^2 + ([\mathbf{Z}^{-1}]_{2,4})^2)$ and $\delta_{\text{DL}} = P_{\text{BS}} M_{\text{UE}} / \sigma_{\eta, \text{UE}}^2$ and $\delta_{\text{UL}} = P_{\text{UE}} M_{\text{BS}} / \sigma_{\eta, \text{BS}}^2$ are the DL and UL receive SNR, respectively. It follows from (31) that the link with the highest receive SNR will provide the best positioning performance. For perfectly synchronized ($\sigma_{\text{clk}}^2 = 0$) or asynchronous ($\sigma_{\text{clk}}^2 \rightarrow \infty$) clocks we have

$$\frac{\text{PEB}^{(\text{DL})}}{\text{PEB}^{(\text{UL})}} = \sqrt{\frac{\delta_{\text{UL}}}{\delta_{\text{DL}}}}. \quad (32)$$

From (31) and (32) we see that DL and UL positioning have different accuracy, owing to different receive SNR. When $\delta_{\text{DL}} = \delta_{\text{UL}}$, again from (31), we find that $\text{PEB}^{(\text{DL})} = \text{PEB}^{(\text{UL})}$. We stress that (31) and (32) hold when each of the devices (BS or UE) employs the same set of orthonormal beamforming vectors for transmission and reception. In case the sets of beamforming vectors for transmission and reception are not the same, there is a mismatch between the subspaces spanned for transmission and reception. Although an analytic result has not been derived for this case, in Section VI, we compare DL and UL positioning using random beamforming matrices for transmission and reception.

V. ASYMPTOTIC ANALYSIS AND GEOMETRIC INTERPRETATION OF FISHER INFORMATION

The expressions for the FIMs and their entries provided in Section III and in Appendix B, although useful for numerical evaluation of the achievable accuracy, do not provide much intuition about the positioning information that is available in the considered single-anchor MIMO-OFDM setup. Our aim is to obtain a geometric interpretation of the Fisher information, as in [13], [18]. Following [17]–[19], we will consider asymptotic expressions for the position and orientation EFIM for large bandwidth³ ($F_s \rightarrow \infty$) and large number of transmit and receive antennas ($N_T, N_R \rightarrow \infty$). The accuracy of the asymptotic expressions has been investigated in [17], where it was shown that they can provide a very accurate approximation of the exact PEB, even for moderate bandwidth and number of transmit and receive antennas.

Since, for arrays with a fixed aperture the asymptotic orthogonality/favorable propagation condition [32], [33] may not be satisfied [34], we consider arrays whose aperture grows with increasing number of elements. In addition to the standard favorable propagation condition

$$\lim_{N_T \rightarrow \infty} \mathbf{a}_{T,p}^H(\tilde{\theta}_{T,l}) \mathbf{a}_{T,p}(\tilde{\theta}_{T,l'}) / N_T = 0, \quad (33)$$

we also assume

$$\lim_{N_T \rightarrow \infty} \frac{\partial}{\partial \tilde{\theta}_{T,l}} \mathbf{a}_{T,p}^H(\tilde{\theta}_{T,l}) \mathbf{a}_{T,p}(\tilde{\theta}_{T,l'}) / N_T^2 = 0, \quad (34)$$

$$\lim_{N_T \rightarrow \infty} \frac{1}{N_T^3} \left\| \partial \mathbf{a}_{T,p}(\tilde{\theta}_{T,l}) / \partial \tilde{\theta}_{T,l} \right\|_2^2 > 0, \quad (35)$$

implying that asymptotic orthogonality holds also for the inner product of the derivative of the array steering vector and the array steering vector at any angle. Similar assumptions are made for the Rx array. We can verify that these conditions hold both for ULAs and UCAs.

In order to focus on the characteristics of the channel and obtain geometrically intuitive expressions for the Fisher information, we also use the following simplifying assumptions:

- 1) $\tilde{g}(t)$ has a flat frequency response over the occupied subcarriers.
- 2) $\mathbf{F}_T = \mathbf{I}_{N_T}$ and $\mathbf{F}_R = \mathbf{I}_{N_R}$, i.e. the whole transmit and receive spaces can be sensed.
- 3) The entries of the reference signal $\mathbf{x}_b[p]$ are assumed to be independent and identically distributed (i.i.d) random variables with $\mathbb{E}[\mathbf{x}_b[p] \mathbf{x}_b^H[p]] = \gamma_p P_T / N_T \mathbf{I}_{N_T}$ and $\mathbb{E}[\mathbf{x}_b[p] \mathbf{x}_b^H[q]] =$

³In an OFDM system with a given number of subcarriers and a fixed set of occupied subcarriers, the occupied bandwidth increases linearly with the sampling rate. Hence, equivalently to writing that the bandwidth goes to infinity we write $F_s \rightarrow \infty$

$\mathbf{0}$, $p \neq q$. Hence, in this section we compute the entries of the FIMs, taking the expectation over the reference signal, as in [18]:

$$\left[\mathbf{J}_\phi^{(o)} \right]_{i,j} = \frac{1}{\sigma_{\eta,R}^2} \sum_{b=1}^{N_B} \sum_{p \in \mathcal{P}} \Re \left\{ \mathbb{E} \left[\frac{\partial \mathbf{m}_b^H[p]}{\partial \phi_i} \frac{\partial \mathbf{m}_b[p]}{\partial \phi_j} \right] \right\}. \quad (36)$$

To make the following expressions more compact we set $d_{T,R} = \|\mathbf{p}_R - \mathbf{p}_T\|_2$, $d_{T,s,l} = \|\mathbf{p}_{s,l} - \mathbf{p}_T\|_2$ and $d_{R,s,l} = \|\mathbf{p}_R - \mathbf{p}_{s,l}\|_2$. As before, we distinguish between the static and dynamic scenario.

A. Static Scenario

Before presenting the main results we define a few useful quantities.

Definition 1: The *effective baseband bandwidth* β of the signal is defined as

$$\beta = \sqrt{\sum_{p \in \mathcal{P}} \gamma_p \omega_p^2 - \left(\sum_{p \in \mathcal{P}} \gamma_p \omega_p \right)^2}. \quad (37)$$

Definition 2: The *effective angular carrier frequency* $\bar{\omega}_c$ of the signal is defined as

$$\bar{\omega}_c = \sqrt{\sum_{p \in \mathcal{P}} \gamma_p (\omega_c + \omega_p)^2}. \quad (38)$$

The definitions in (37) and (38) are the multi-carrier counterparts of the effective baseband bandwidth and the effective carrier frequency defined in [13] for single-carrier systems.

Definition 3: The *squared array aperture function* (SAAF) of the Tx array is defined as [13]

$$S_T(\tilde{\theta}_{T,l}) = \frac{1}{N_T} \sum_{j=1}^{N_T} \left(d_{T,j} \mathbf{u}_\perp(\psi_{T,j}) \mathbf{u}(\tilde{\theta}_{T,l}) \right)^2, \quad (39)$$

where $\mathbf{u}_\perp(\psi) = \mathbf{u}(\psi - \pi/2)$, with the array's centroid chosen at its reference point. The SAAF of the Rx array is defined accordingly. The Tx (Rx) SAAF fully describes the effect of the Tx (Rx) array structure on the AOD (AOA) information.

Theorem 1: (Static receiver localization) The EFIM for the position \mathbf{p}_R and orientation α_R of an imperfectly synchronized static receiver, when the position \mathbf{p}_T and orientation α_T of the transmitter are known, can be asymptotically expressed as

$$\mathbf{J}_{\text{po}}^{(s)} \rightarrow \begin{cases} \delta_{R,T} \left(\mathbf{J}_{\text{LOS}}^{(s)} + \sum_{l=1}^{L-1} \mathbf{J}_{\text{NLOS},l}^{(s)} - \mathbf{J}_{\text{clk}}^{(s)} \right), & \text{if LOS exists,} \\ \delta_{R,T} \left(\sum_{l=0}^{L-1} \mathbf{J}_{\text{NLOS},l}^{(s)} - \mathbf{J}_{\text{clk}}^{(s)} \right), & \text{otherwise,} \end{cases} \quad (40)$$

where $\delta_{R,T} = N_R N_B P_T / \sigma_{\eta,R}^2$ is the receive SNR. The information from the LOS path is given by

$$\mathbf{J}_{\text{LOS}}^{(s)} = |h_0|^2 \left[\frac{\beta^2}{c^2} \mathbf{z}_{\tau_0} \mathbf{z}_{\tau_0}^T + \frac{\bar{\omega}_c^2}{c^2 d_{T,R}^2} \left(S_T(\tilde{\theta}_{T,0}) \mathbf{z}_{\theta_{T,0}} \mathbf{z}_{\theta_{T,0}}^T + S_R(\tilde{\theta}_{R,0}) \mathbf{z}_{\theta_{R,0}} \mathbf{z}_{\theta_{R,0}}^T \right) \right], \quad (41)$$

with $\mathbf{z}_{\tau_0} = [-\mathbf{u}^T(\theta_{R,0}), 0]^T$, $\mathbf{z}_{\theta_{T,0}} = [\mathbf{u}_\perp^T(\theta_{R,0}), 0]^T$ and $\mathbf{z}_{\theta_{R,0}} = [\mathbf{u}_\perp^T(\theta_{R,0}), -d_{T,R}]^T$. The information from the l -th NLOS path is described by

$$\mathbf{J}_{\text{NLOS},l}^{(s)} = |h_l|^2 f_l \mathbf{z}_l \mathbf{z}_l^T, \quad (42)$$

with

$$f_l = \left(\frac{c^2 (1 + \cos(\Delta\theta_l))^2}{\bar{\omega}_c^2} \left(\frac{d_{T,s,l}^2}{S_T(\tilde{\theta}_{T,l})} + \frac{d_{R,s,l}^2}{S_R(\tilde{\theta}_{R,l})} \right) + \frac{\sin^2(\Delta\theta_l) c^2}{\beta^2} \right)^{-1}, \quad (43)$$

$$\mathbf{z}_l = \left[\mathbf{u}_\perp^T(\theta_{T,l}) + \mathbf{u}_\perp^T(\theta_{R,l}), \quad -(1 + \cos(\Delta\theta_l)) d_{R,s,l} \right]^T \in \mathbb{R}^3, \quad (44)$$

and the information loss due to the synchronization error, is described by

$$\mathbf{J}_{\epsilon_{\text{clk}}}^{(s)} = \mathbf{z}_{\epsilon_{\text{clk}}} \mathbf{z}_{\epsilon_{\text{clk}}}^T / K_{\epsilon_{\text{clk}}}, \quad (45)$$

where

$$\mathbf{z}_{\epsilon_{\text{clk}}} = \begin{cases} |h_0|^2 \frac{\beta^2}{c^2} \mathbf{z}_{\tau_0} + \sum_{l=1}^L |h_l|^2 \sin(\Delta\theta_l) f_l \mathbf{z}_l, & \text{if LOS exists,} \\ \sum_{l=0}^L |h_l|^2 \sin(\Delta\theta_l) f_l \mathbf{z}_l, & \text{otherwise,} \end{cases} \quad (46)$$

$$K_{\epsilon_{\text{clk}}} = \begin{cases} \frac{1}{\delta_{R,T} \sigma_{\text{clk}}^2} + |h_0|^2 \frac{\beta^2}{c^2} + \sum_{l'=1}^{L-1} |h_{l'}|^2 \sin^2(\Delta\theta_{l'}) f_{l'}, & \text{if LOS exists,} \\ \frac{1}{\delta_{R,T} \sigma_{\text{clk}}^2} + \sum_{l'=0}^{L-1} |h_{l'}|^2 \sin^2(\Delta\theta_{l'}) f_{l'}, & \text{otherwise.} \end{cases} \quad (47)$$

Proof: See Appendix C. ■

Some interesting remarks are to be made based on Theorem 1. Similar to [18], we find that the EFIM of each of the single-bounce NLOS paths is rank-1. We can also see from (42) and (44) that the direction of the position information offered by a single-bounce NLOS path is determined solely by the geometry and is independent of the system parameters. The direction is given by the sum of the 2D unit vectors pointing to the directions orthogonal to the AOD and AOA of the NLOS path.

We observe that, in the LOS-only case, where the derived expressions (40),(41), (45)-(47) are exact, for an imperfectly synchronized system ($0 < \sigma_{\text{clk}}^2 < \infty$) positioning is possible. However, the ranging information provided by the TOA of the LOS path decreases with increasing σ_{clk} and the achievable positioning accuracy is lower bounded by the synchronization error-induced ranging error $\sigma_{\text{clk}} c$. Hence, large values of σ_{clk} may lead to poor position estimation accuracy. For an asynchronous system ($\sigma_{\text{clk}}^2 \rightarrow \infty$), the ranging information from the TOA of the LOS path vanishes entirely and at least one NLOS path in addition to the LOS path is required.

When there is no LOS path, at least three NLOS paths are required for positioning [18]. Similarly to the LOS-only case, the achievable accuracy is lower bounded by $\sigma_{\text{clk}}c$ and for an asynchronous system an additional NLOS path is required for positioning.

Similar results can be obtained for unknown Tx position and orientation:

Theorem 2: (Static transmitter localization) The EFIM for the position \mathbf{p}_T and the orientation α_T of an imperfectly synchronized transmitter, when the position \mathbf{p}_R and orientation α_R of the receiver are known, can be asymptotically expressed as in (40), (41), (42) and (45), with $\mathbf{z}_{\tau_0} = [-\mathbf{u}^T(\theta_{T,0}), 0]^T \in \mathbb{R}^3$, $\mathbf{z}_{\theta_{T,0}} = [\mathbf{u}_\perp^T(\theta_{T,0}), -d_{T,R}]^T$, $\mathbf{z}_{\theta_{R,0}} = [\mathbf{u}_\perp^T(\theta_{T,0}), 0]^T$, and $\mathbf{z}_l = [\mathbf{u}_\perp^T(\theta_{T,l}) + \mathbf{u}_\perp^T(\theta_{R,l}), -(1 + \cos(\Delta\theta_l))d_{T,s,l}]^T$.

Proof: Similar to the proof of Theorem 1. ■

Theorems 1 and 2 can be used for the analysis of the effect of the geometry and the system parameters on the DL and UL positioning accuracy, respectively. Theorem 2 can also be used for the analysis of sidelink positioning, where a UE estimates another UE's relative position.

B. Dynamic Scenario

In order to keep the expressions relatively simple and gain insight on the effect of the movement of the receiver or the transmitter, apart from the assumptions made for the static scenario, we additionally assume that $\omega_c \gg \omega_p$, $p \in \mathcal{P}$, in other words that the system under consideration is narrowband. Again, before presenting the results, we define a couple of useful quantities.

Definition 4: The *effective baseband bandwidth* of the signal arriving from the l -th path is

$$\beta_l = \sqrt{\sum_{q \in \mathcal{P}} \xi_{l,q} \gamma_q \omega_q^2 / \xi_l - \left(\sum_{q \in \mathcal{P}} \xi_{l,q} \gamma_q \omega_q / \xi_l \right)^2}, \quad (48)$$

where $\xi_{l,q} = \sum_{p \in \mathcal{P}} |Q(\Phi_{p,q,l})|^2$ describes the intensity effect of the Doppler shift for the l -th path on the q -th subcarrier and $\xi_l = \sum_{q \in \mathcal{P}} \gamma_q \xi_{l,q}$, with $\Phi_{p,q,l} = (\omega_p - \omega_q - v_l \omega_c / c) T_s / 2$. Similar to what is reported in [13], the intensity effect for mm-Wave systems with large bandwidth is very small and can be neglected, i.e. $\xi_{l,q} \approx 1$, l, q . Then, (48) falls back to (37) $\forall l$.

Definition 5: The *root mean square (rms) duration* of the reference signal arriving from the l -th path is

$$t_{\text{rms},l} = T_s \sqrt{M^2 (N_B^2 - 1) / 12 + n_{\text{B,rms},l}^2}, \quad (49)$$

where

$$n_{\text{B,rms},l}^2 = \frac{\sum_{q \in \mathcal{P}} \gamma_q \sum_{p \in \mathcal{P}} |Q(\Phi_{p,q,l})|^2 (\cot(\Phi_{p,q,l}) - N \cot(N\Phi_{p,q,l}))^2 / 4}{\xi_l} - \left(\frac{\sum_{q \in \mathcal{P}} \gamma_q \sum_{p \in \mathcal{P}} |Q(\Phi_{p,q,l})|^2 (\cot(\Phi_{p,q,l}) - N \cot(N\Phi_{p,q,l})) / 2}{\xi_l} \right)^2. \quad (50)$$

It can be shown that for practical scenarios with $\|\mathbf{v}_R\|_2/c \ll 1$

$$n_{\text{B,rms},l}^2 \approx n_{\text{B,rms}}^2 = \sum_{q \in \mathcal{P}} \gamma_q \sum_{p \in \mathcal{P}, p \neq q} \sin^{-2}(\pi(p-q)/N). \quad (51)$$

We now present the main result for the dynamic scenario:

Theorem 3: (Mobile receiver localization) The EFIM for the position \mathbf{p}_R , orientation α_R and velocity \mathbf{v}_R of an imperfectly synchronized mobile receiver, when the position \mathbf{p}_T and orientation α_T of the static transmitter are known, can be asymptotically expressed as

$$\mathbf{J}_{\text{pov}}^{(d)} \rightarrow \begin{cases} \delta_{R,T} \left(\mathbf{J}_{\text{LOS}}^{(d)} + \sum_{l=1}^{L-1} \mathbf{J}_{\text{NLOS},l}^{(d)} - \mathbf{J}_{\epsilon_{\text{clk}}}^{(d)} \right), & \text{if LOS exists,} \\ \delta_{R,T} \left(\sum_{l=1}^{L-1} \mathbf{J}_{\text{NLOS},l}^{(d)} - \mathbf{J}_{\epsilon_{\text{clk}}}^{(d)} \right), & \text{otherwise,} \end{cases} \quad (52)$$

where the information from the LOS path is described by

$$\mathbf{J}_{\text{LOS}}^{(d)} = |h_0|^2 \xi_0 \left[\frac{\beta_0^2}{c^2} \mathbf{z}_{\tau_0} \mathbf{z}_{\tau_0}^T + \frac{\omega_c^2}{c^2 d_{T,R}^2} \left(S_T(\tilde{\theta}_{T,0}) \mathbf{z}_{\theta_{T,0}} \mathbf{z}_{\theta_{T,0}}^T + S_R(\tilde{\theta}_{R,0}) \mathbf{z}_{\theta_{R,0}} \mathbf{z}_{\theta_{R,0}}^T + \rho_0^2 t_{\text{rms},0}^2 \mathbf{z}_{v_0} \mathbf{z}_{v_0}^T \right) \right], \quad (53)$$

with

$$\mathbf{z}_{\tau_0} = [-\mathbf{u}^T(\theta_{R,0}), 0, 0, 0]^T \in \mathbb{R}^5, \quad (54)$$

$$\mathbf{z}_{\theta_{T,0}} = [\mathbf{u}_{\perp}^T(\theta_{R,0}), 0, 0, 0]^T \in \mathbb{R}^5, \quad (55)$$

$$\mathbf{z}_{\theta_{R,0}} = [\mathbf{u}_{\perp}^T(\theta_{R,0}), -d_{T,R}, 0, 0]^T \in \mathbb{R}^5, \quad (56)$$

$$\mathbf{z}_{v_0} = [-\mathbf{u}_{\perp}^T(\theta_{R,0}), 0, d_{T,R} \mathbf{u}^T(\theta_{R,0}) / \rho_0]^T \in \mathbb{R}^5, \quad (57)$$

and $\rho_l = \mathbf{v}_R^T \mathbf{u}_{\perp}(\theta_{R,l})$, $l = 0, \dots, L-1$, being the transverse velocity component. The information from the l -th NLOS path neglecting its coupling with other paths is described by

$$\mathbf{J}_{\text{NLOS},l}^{(d)} = |h_l|^2 \xi_l (f_{\tau,\theta,l} \mathbf{z}_{\tau,\theta,l} \mathbf{z}_{\tau,\theta,l}^T + f_{\tau,v,l} \mathbf{z}_{\tau,v,l} \mathbf{z}_{\tau,v,l}^T + f_{\theta,v,l} \mathbf{z}_{\theta,v,l} \mathbf{z}_{\theta,v,l}^T), \quad (58)$$

with

$$\mathbf{z}_{\tau,\theta,l} = [\mathbf{u}_{\perp}^T(\theta_{T,l}) + \mathbf{u}_{\perp}^T(\theta_{R,l}), -(1 + \cos(\Delta\theta_l)) d_{R,s,l}, 0, 0]^T \in \mathbb{R}^5, \quad (59)$$

$$\mathbf{z}_{\theta,v,l} = [0, 0, -d_{R,s,l}, d_{R,s,l} \mathbf{u}^T(\theta_{R,l}) / \rho_l]^T \in \mathbb{R}^5, \quad (60)$$

$$\mathbf{z}_{\tau,v,l} = \mathbf{z}_{\tau,\theta,l} - (1 + \cos(\Delta\theta_l)) \mathbf{z}_{\theta,v,l}, \quad (61)$$

and

$$\begin{aligned}
f_{\tau,\theta,l} &= \frac{i_{\tau_l} i_{\theta_{R,l}} i_{\theta_{T,l}}}{\chi_l}, \quad f_{\tau,v,l} = \frac{i_{\tau_l} i_{v_l} i_{\theta_{T,l}}}{\chi_l}, \quad f_{\theta,v,l} = \frac{i_{\theta_{R,l}} i_{v_l}}{\chi_l} (i_{\tau_l} (1 + \cos(\Delta\theta_l))^2 + i_{\theta_{T,l}} \sin^2(\Delta\theta_l)), \\
\chi_l &= (1 + \cos(\Delta\theta_l))^2 i_{\tau_l} (i_{\theta_{T,l}} + i_{\theta_{R,l}} + i_{v_l}) + \sin^2(\Delta\theta_l) i_{\theta_{T,l}} (i_{\theta_{R,l}} + i_{v_l}), \\
i_{\tau_l} &= \frac{\beta_l^2}{c^2}, \quad i_{\theta_{T,l}} = \frac{\omega_c^2 S_T(\tilde{\theta}_{T,l})}{c^2 d_{T,s,l}^2}, \quad i_{\theta_{R,l}} = \frac{\omega_c^2 S_R(\tilde{\theta}_{R,l})}{c^2 d_{R,s,l}^2}, \quad i_{v_l} = \frac{\omega_c^2 \rho_l^2 t_{\text{rms},l}^2}{c^2 d_{R,s,l}^2}.
\end{aligned} \tag{62}$$

The information loss due to the synchronization error is described by

$$\mathbf{J}_{\epsilon_{\text{clk}}}^{(d)} = \mathbf{z}_{\epsilon_{\text{clk}}} \mathbf{z}_{\epsilon_{\text{clk}}}^T / K_{\epsilon_{\text{clk}}}, \tag{63}$$

where

$$\begin{aligned}
\mathbf{z}_{\epsilon_{\text{clk}}} &= \begin{cases} \frac{\beta_0^2}{c^2} \xi_0 \mathbf{z}_{\tau_0} + \sum_{l=1}^L |h_l|^2 \sin(\Delta\theta_l) \xi_l ((f_{\tau,\theta,l} + f_{\tau,v,l}) \mathbf{z}_{\tau,\theta,l} + f_{\tau,v,l} \mathbf{z}_{\tau,v,l}), & \text{if LOS exists,} \\ \sum_{l=0}^L |h_l|^2 \sin(\Delta\theta_l) \xi_l (f_{\tau,\theta,l} \mathbf{z}_{\tau,\theta,l} + f_{\tau,v,l} \mathbf{z}_{\tau,v,l}), & \text{otherwise,} \end{cases} \\
K_{\epsilon_{\text{clk}}} &= \begin{cases} \frac{1}{\delta_{R,T} \sigma_{\text{clk}}^2} + |h_0|^2 \frac{\beta_0^2}{c^2} \xi_0 + \sum_{l'=1}^{L-1} |h_{l'}|^2 \xi_{l'} \sin^2(\Delta\theta_{l'}) (f_{\tau,\theta,l} + f_{\tau,v,l}), & \text{if LOS exists,} \\ \frac{1}{\delta_{R,T} \sigma_{\text{clk}}^2} + \sum_{l'=0}^{L-1} |h_{l'}|^2 \xi_{l'} \sin^2(\Delta\theta_{l'}) (f_{\tau,\theta,l} + f_{\tau,v,l}), & \text{otherwise.} \end{cases}
\end{aligned}$$

Proof: Similar to the proof of Theorem 1. ■

Some remarks on the theorem above should be made. From (57), we see that the Doppler shift of the LOS offers velocity information in the radial direction. In addition, it provides position information in the transverse direction, which corresponds to angle information. The intuition behind this is that, as an antenna array provides angle information by sampling the space at different locations *simultaneously*, the movement of the receiver also provides angle information by allowing every single antenna element to sample the space at different locations *over time*. The intensity of the position information is proportional to $\rho_0^2 t_{\text{rms},0}^2$. As explained in [13], $\rho_0 t_{\text{rms},0}$ can be interpreted as the *synthetic array aperture* for the LOS path, which is generated by the movement of the receiver.

For the l -th single-bounce NLOS path the synthetic array aperture is $\rho_l t_{\text{rms},l}$. From (58)-(61) we conclude that, from rank-1 Fisher information in \mathbb{R}^3 in the static scenario, the single-bounce NLOS paths now offer rank-2 information in \mathbb{R}^5 . This results from the fact that $\mathbf{z}_{\tau,v,l}$ is a linear combination of $\mathbf{z}_{\tau,\theta,l}$ and $\mathbf{z}_{\theta,v,l}$. The EFIM from the l -th path is composed by the three rank-1 matrices determined by $\mathbf{z}_{\tau,\theta,l}$, $\mathbf{z}_{\tau,v,l}$ and $\mathbf{z}_{\theta,v,l}$. Only the first two matrices offer position information, in the same direction as in the static scenario. More specifically, the first matrix offers position and orientation information and the second matrix position and velocity

information. The third matrix contains information only about the orientation and the velocity of the receiver.

In case the LOS path exists, at least one NLOS path is additionally required to have a full rank \mathbf{J}_{pov} , i.e. in order to be able to estimate the position, orientation and velocity. When only the LOS path is available, the transverse velocity cannot be estimated. Writing $\mathbf{v}_R = v_r \mathbf{u}(\theta_{R,0}) + v_\perp \mathbf{u}(\theta_{R,0} + \pi/2)$, where v_r and v_\perp are the radial and transverse velocity components, and plugging it into the dynamic signal model (10), (11), we can see that only the radial velocity is observable. This could also be seen from (57), where we observe that the LOS path offers velocity information only in the radial direction. Therefore, the LOS path allows us to estimate the position and the radial velocity v_r , but the NLOS paths enable us to obtain the missing orthogonal component v_\perp of the velocity vector. This could be very important in the prediction step of position tracking algorithms. In the NLOS-only case three paths are required to obtain the position, orientation and velocity of the receiver, even in asynchronous operation.

Similar results, which are omitted for brevity, can be obtained in the case with a moving transmitter with unknown orientation and a static receiver (*mobile transmitter localization*).

VI. NUMERICAL RESULTS

In this section, we numerically evaluate the expressions derived above. First, we study the effect of synchronization errors on the achievable positioning accuracy. Then, we investigate the impact of mobility on the PEB for different channel types (LOS-only, NLOS-only, LOS + NLOS) and different levels of synchronization error variance. Finally, we conduct a DL and UL positioning comparison with random beamformers.

A. Simulation parameters

For the channel model we follow [18]: the magnitude of the coefficient of the LOS path is $|h_0| = \lambda_c / (4\pi d_{T,R})$, the magnitude of the NLOS paths, which are assumed to come from reflections, is $|h_l| = \Gamma_{\text{refl}} \lambda_c / (4\pi (d_{T,s,l} + d_{R,s,l}))$ with $\Gamma_{\text{refl}} = 0.1$, and the phase of all the paths is uniformly distributed.

We consider a setup where the transmitter and the receiver are equipped with UCAs with $\lambda_c/2$ -spaced elements, where $\lambda_c = c/f_c$ with $f_c = 38$ GHz. The orientation of the arrays is irrelevant as the SAAF of a UCA is independent of the angle. Unless otherwise specified, we set $N_T = N_R = 32$. and fix the position of the transmitter at $\mathbf{p}_T = [0 \text{ m}, 0 \text{ m}]^T$, the position of the

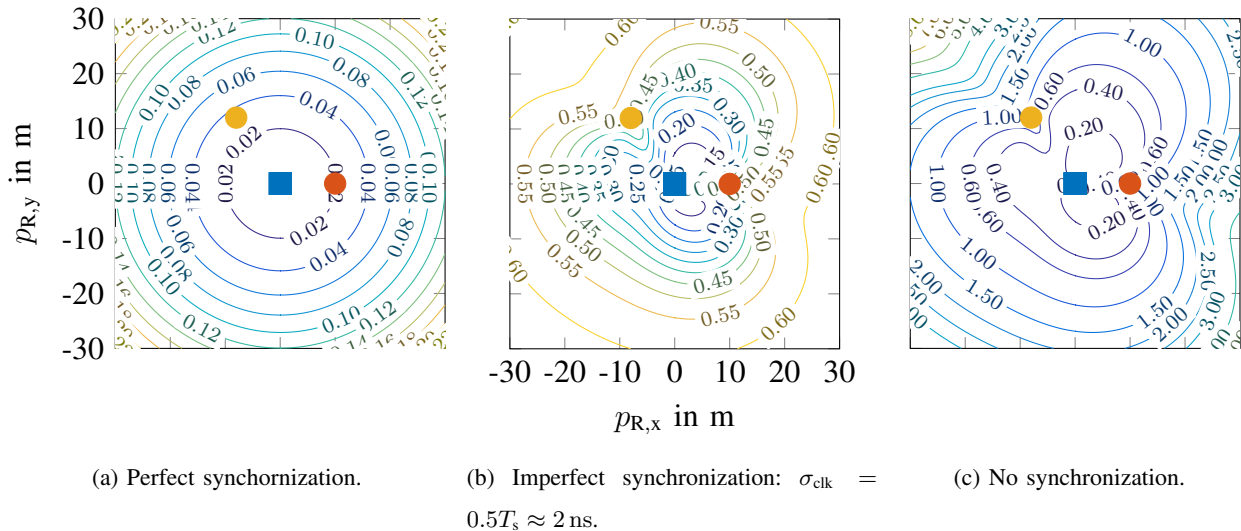


Fig. 2. PEB in m for receiver localization with $\mathbf{p}_T = [0 \text{ m}, 0 \text{ m}]^T$, $\mathbf{p}_{s,1} = [10 \text{ m}, 0 \text{ m}]^T$ and $\mathbf{p}_{s,2} = [-8 \text{ m}, 12 \text{ m}]^T$ under different levels of synchronization error variance. The position of the transmitter is shown with a square and the positions of the reflectors with circles.

reflectors at $\mathbf{p}_{s,1} = [10 \text{ m}, 0 \text{ m}]^T$ and $\mathbf{p}_{s,2} = [-8 \text{ m}, 12 \text{ m}]^T$. The receiver lies in a $60 \text{ m} \times 60 \text{ m}$ area with the transmitter at its center, i.e. $-30 \text{ m} \leq p_{R,x} \leq 30 \text{ m}$, $-30 \text{ m} \leq p_{R,y} \leq 30 \text{ m}$. The sampling frequency is set to $F_s = 245.76 \text{ MHz}$ and the DFT size is $N = 1024$, resulting in a subcarrier spacing of 240 kHz . One OFDM symbol is transmitted ($N_B = 1$), where the set of occupied subcarriers is $\mathcal{P} = \{-297, -291, \dots, 291, 297\}$ and $\gamma_p = 1/|\mathcal{P}|$, $\forall p \in \mathcal{P}$, with $|\mathcal{P}| = 100$. The power per subcarrier is 0 dBm , thus $P_T = 20 \text{ dBm}$. The noise spectral density is $N_0 = -170 \text{ dBm Hz}^{-1}$.

B. The importance of synchronization

We now compare systems with or without synchronization errors for receiver localization. In Fig. 2 we plot the asymptotic PEB for a receiver with perfect synchronization (Fig. 2(a)), with imperfect synchronization with $\sigma_{\text{clk}} = 0.5T_s \approx 2 \text{ ns}$ (Fig. 2(b)), and without synchronization (Fig. 2(c)). Sub-meter positioning accuracy is attainable for all the considered receiver locations, when perfect synchronization or imperfect synchronization with $\sigma_{\text{clk}} = 0.5T_s$ is available. However, in asynchronous operation (Fig. 2(c)), there is significant accuracy degradation because the positioning information from the LOS is no longer sufficient and information from the much weaker NLOS paths is required to compute the position. We can see in Fig. 2(b) that clock

synchronization errors with standard deviation as small as $0.5T_s \approx 2 \text{ ns}$ can severely degrade the achievable positioning accuracy, compared to the case with perfect synchronization.

We observe in Fig. 2 that with perfect synchronization the PEB depends only on the distance from the transmitter, as the contour lines are concentric circles with the transmitter at their center. This is attributed to the fact that the distance and angle information from the LOS path are dominant. With imperfect or no synchronization, the distance information from the LOS path is significantly reduced or vanished. The information offered by the NLOS paths, especially the information in the radial direction, allows the receiver to resolve the synchronization error and hence compute its distance from the transmitter more accurately. Since the direction and the intensity of the information from each NLOS path depends on the relative position of the receiver with respect to the reflector (see (43) and (44)), the contour lines in Figs. 2(b) and 2(c) are influenced not only by the position of the transmitter but also from the position of the reflectors. A characteristic example is when the receiver lies in the area behind a reflector. In this case $\mathbf{u}_\perp(\theta_{T,l}) \approx -\mathbf{u}_\perp(\theta_{R,l})$ and, thus, from (44) we can conclude that the information offered by the corresponding path is significantly reduced. This explains the curvature of the contour lines in the regions behind the reflectors.

In order to further study the effect of synchronization on positioning accuracy, in Fig. 3 we plot the PEB as a function of σ_{clk}/T_s with the receiver's position fixed at $\mathbf{p}_R = [18 \text{ m}, 3 \text{ m}]^T$. To also evaluate the performance of NLOS-only positioning, which requires at least 4 paths in the asynchronous case, we add extra reflectors at $\mathbf{p}_{s,3} = [12 \text{ m}, 8 \text{ m}]^T$ and $\mathbf{p}_{s,4} = [7 \text{ m}, -6 \text{ m}]^T$. The following 5 cases are considered: (i) *LOS-only*: only the LOS path is available; (ii) *3 NLOS-only*: only 3 NLOS paths (corresponding to $\mathbf{p}_{s,1}$, $\mathbf{p}_{s,2}$ and $\mathbf{p}_{s,3}$) are available; (iii) *LOS + 3 NLOS*: the LOS and the 3 NLOS paths are available; (iv) *4 NLOS-only*: only 4 NLOS paths are available; (v) *LOS + 4 NLOS*: the LOS and the 4 NLOS paths are available. In the LOS-only case and in the NLOS-only case with 3 NLOS paths, the accuracy is significantly degraded with increasing σ_{clk} , as the performance of these cases is lower-bounded by the standard deviation of the ranging error caused by the synchronization error, which is equal to $\sigma_{\text{clk}}c$ (see also the discussion after Theorem 1). On the other hand, with 4 NLOS paths, the PEB of NLOS-only positioning saturates with increasing σ_{clk} , as the synchronization error can be resolved using the paths. Similarly, when both LOS and NLOS paths are present the PEB saturates, with the saturation value improving with increasing number of paths.

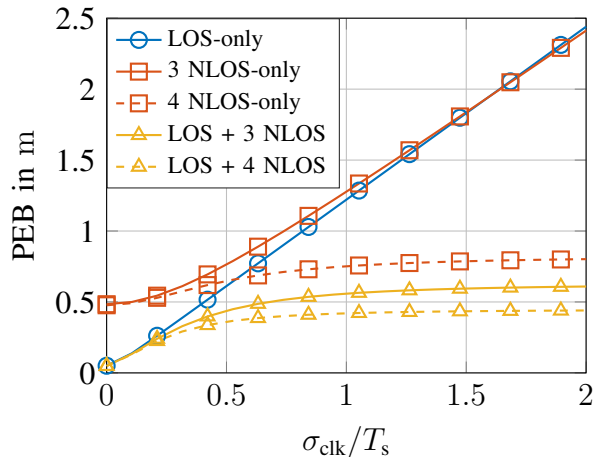


Fig. 3. PEB vs σ_{clk} for LOS and NLOS static receiver localization with $\mathbf{p}_T = [0 \text{ m}, 0 \text{ m}]^T$, $\mathbf{p}_R = [18 \text{ m}, 3 \text{ m}]^T$, $\mathbf{p}_{s,1} = [10 \text{ m}, 0 \text{ m}]^T$, $\mathbf{p}_{s,2} = [-8 \text{ m}, 12 \text{ m}]^T$, $\mathbf{p}_{s,3} = [12 \text{ m}, 8 \text{ m}]^T$, $\mathbf{p}_{s,4} = [7 \text{ m}, -6 \text{ m}]^T$.

C. The effect of Doppler shifts

We consider the setup described in Section VI-A, but the receiver is now moving with velocity $\mathbf{v}_R = \mathbf{u}(\pi/2)60 \text{ km h}^{-1}$. Instead of 1 OFDM symbol, we now transmit $N_B = 32$ OFDM symbols, such that the synthetic array aperture is comparable to the physical aperture of the antenna arrays. The duration of the CP is $72T_s \approx 0.07NT_s$. We keep the total transmit power the same as in the static scenario, i.e. $N_B P_T = 20 \text{ dBm}$, so as to observe the effect of the receiver's movement for the same receive SNR. We can see in Fig. 4 that, compared to the static case, no considerable improvement is achieved except for the areas behind the reflectors. As explained in the discussion of Fig. 2, in these regions, the movement-independent part of the information from the corresponding NLOS path (see (58),(59)) is reduced. Therefore, the additional information offered by the Doppler shift (see (58), (60), (61)) becomes important.

To gain further insight on the effect of velocity, in Fig. 5 we plot the PEB as a function of the speed, i.e. $\|\mathbf{v}_R\|_2$, for a system with perfect ($\sigma_{\text{clk}} = 0$) and imperfect ($\sigma_{\text{clk}} = 2T_s$) synchronization. Again, we fix the receiver's position at $\mathbf{p}_R = [18 \text{ m}, 3 \text{ m}]^T$ and add an extra reflector at $\mathbf{p}_{s,3} = [12 \text{ m}, 8 \text{ m}]^T$. We consider three different cases: (i) *LOS-only*: only the LOS path is available; (ii) *NLOS-only*: only the 3 NLOS paths are available; (iii) *LOS+NLOS*: the LOS and the 3 NLOS paths are available. A few interesting observations can be made from Fig. 5. In the perfectly synchronized system ($\sigma_{\text{clk}} = 0$) the position information offered by the LOS path is dominant and the information from the NLOS path does not improve the PEB (LOS-only

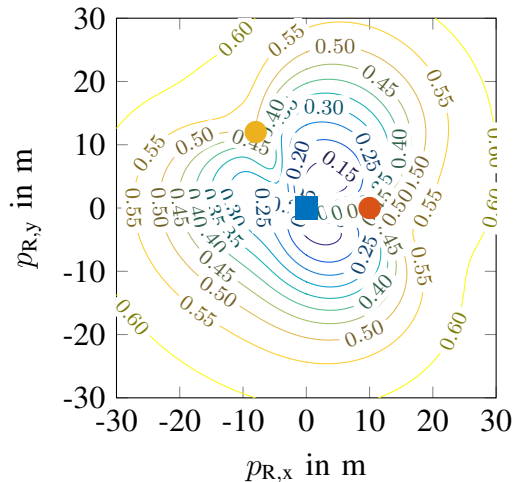


Fig. 4. PEB in m for receiver localization with $\mathbf{p}_T = [0 \text{ m}, 0 \text{ m}]^T$, $\mathbf{p}_{s,1} = [10 \text{ m}, 0 \text{ m}]^T$ and $\mathbf{p}_{s,2} = [-8 \text{ m}, 12 \text{ m}]^T$, receiver velocity $\mathbf{v}_R = \mathbf{u}(\pi/2)60 \text{ km h}^{-1}$, $\sigma_{\text{clk}} = 0.5T_s \approx 2 \text{ ns}$. The position of the transmitter is shown with a square and the positions of the reflectors with circles.

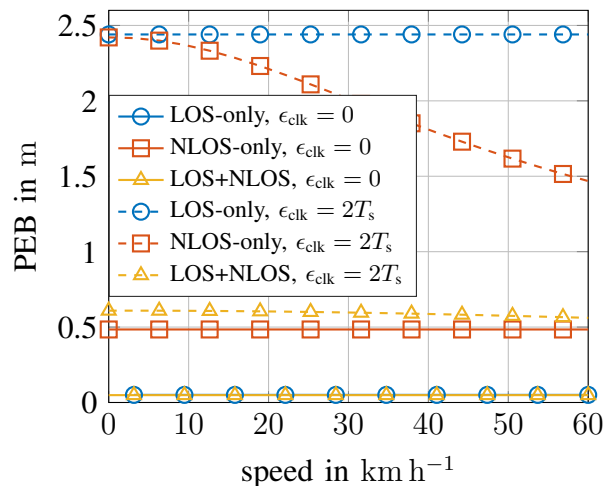


Fig. 5. PEB vs speed for LOS and NLOS receiver localization for perfect ($\sigma_{\text{clk}} = 0$) and imperfect synchronization ($\sigma_{\text{clk}} = 2T_s$) with $\mathbf{p}_T = [0 \text{ m}, 0 \text{ m}]$, $\mathbf{p}_R = [18 \text{ m}, 3 \text{ m}]^T$, $\mathbf{p}_{s,1} = [10 \text{ m}, 0 \text{ m}]^T$ and $\mathbf{p}_{s,2} = [-8 \text{ m}, 12 \text{ m}]^T$, $\mathbf{p}_{s,3} = [12 \text{ m}, 8 \text{ m}]^T$, velocity direction $\mathbf{v}_R / \|\mathbf{v}_R\|_2 = \mathbf{u}(\pi/2)$.

and LOS+NLOS curves coincide). In addition, the movement of the receiver does not improve the positioning accuracy in any of the three considered cases. In the imperfectly synchronized system ($\sigma_{\text{clk}} = 2T_s$), the accuracy of the LOS-only case is lower bounded by the standard deviation $\sigma_{\text{clk}c} \approx 2.44 \text{ m}$ of the ranging error induced by the synchronization error. From the LOS+NLOS curves, we first observe that the information from the NLOS paths is very important

as it allows the receiver to resolve the synchronization error, as discussed before. Similarly to Fig. 4, we can see that the movement of the receiver has a small impact on the PEB, when the LOS path is present. On the contrary, in the NLOS-only case, mobility has a strong impact, with the PEB decreasing significantly with increasing speed. This can be understood by comparing (42)-(44) with (58)-(61): the additional sources of position and orientation information (2nd and 3rd matrices in (58)), whose intensities are proportional to ρ_t^2 , allow the receiver to better resolve the synchronization error, while in the static scenario its accuracy is bounded by $\sigma_{\text{clk}}c$.

D. Comparison of Uplink and Downlink Positioning

In Section IV, we studied the relation of the PEB in the DL and the UL when the same set of orthonormal beamforming vectors are used by each device for transmission and reception. We found that, under the same receive SNR, DL and UL positioning are equivalent. Here, we conduct a numerical comparison of DL and UL positioning when the devices employ random beamforming vectors for transmission and reception. We consider the same setup as before, with perfect synchronization, but we now consider LOS-only propagation and set $M_{\text{BS}} = 16$, which is M_{T} in the DL and M_{R} in the UL. Similarly, we set $M_{\text{UE}} = 4$, which is M_{R} in the DL and M_{T} in the UL. At each considered UE position, the entries of all beamforming matrices are unimodular with random phase uniformly distributed in $[-\pi, \pi)$. The available transmit power is uniformly allocated to the beamforming vectors and the subcarriers, i.e. $\sum_{b=0}^{N_{\text{B}}-1} \mathbf{s}_b[p] \mathbf{s}_b^{\text{H}}[p] = N_{\text{B}} P_{\text{T}} / (M_{\text{T}} |\mathcal{P}|) \mathbf{I}_{M_{\text{T}}}$. Motivated by our findings about the relation between DL and UL positioning in Section IV, we set $\sigma_{\eta, \text{UE}}^2 = 2\sigma_{\eta, \text{BS}}^2$ and $P_{\text{UE}} = P_{\text{BS}} \frac{\sigma_{\eta, \text{BS}}^2 M_{\text{UE}}}{\sigma_{\eta, \text{UE}}^2 M_{\text{BS}}}$, which leads to the same receive SNR in the DL and the UL, with $N_{\text{B}} P_{\text{BS}} = 20$ dBm and the noise spectral density of the BS $N_{0, \text{BS}} = -170$ dBm Hz⁻¹. In Fig. 6, using the expressions for the exact CRLB (13)-(15), (21), (22), we plot the cumulative distribution function (cdf) for the PEB in the DL and UL for $\alpha_{\text{UE}} = 180^\circ$. We can observe in Fig. 6 that, under the same receive SNR, the DL and UL PEB are approximately equal, similarly to the case of orthonormal beamforming. In general, the link with the highest receive SNR will provide the best performance.

VII. CONCLUSION

We derived asymptotic expressions for the Fisher information on position, orientation and velocity for transmitter and receiver localization in a MIMO-OFDM setup, considering synchronization errors and mobility of the transmitter or receiver. We studied the impact of syn-

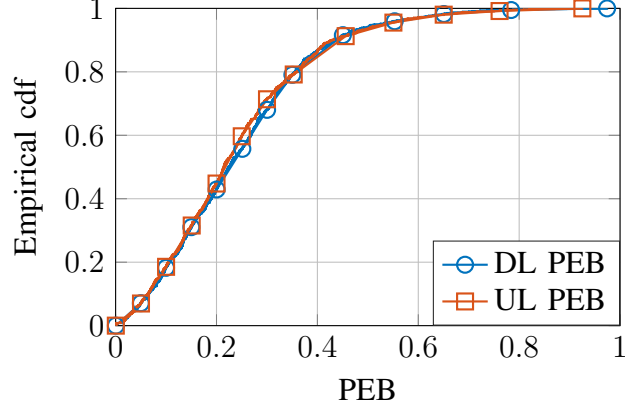


Fig. 6. DL and UL positioning comparison with random beamforming vectors for transmission and reception.

chronization errors and found that even small synchronization errors can significantly degrade the achievable positioning accuracy. Through analytical and numerical results we showed that NLOS paths can help resolve the clock offset and drastically improve the PEB. In addition, we investigated the effect of mobility and proved that each single-bounce NLOS path offers rank-2 information on position, orientation and velocity. Our numerical results showed that in the presence of the LOS path mobility has no significant impact on the achievable positioning accuracy. However, for NLOS-only positioning, it can provide valuable information that can drastically improve the positioning accuracy of an imperfectly synchronized system. Finally, we compared DL and UL positioning with orthonormal or random beamforming and found that they are equivalent when the DL and UL receive SNR are equal.

APPENDIX A

DERIVATIVES OF $\mathbf{m}_b[p]$ W.R.T. THE PARAMETERS IN THE CHANNEL PARAMETER VECTOR

We provide the required derivatives of $\mathbf{m}_b[p]$ for the dynamic scenario; the required derivatives for the static scenario can be obtained from them by setting $\mathbf{v}_R = \mathbf{0}$ (or equivalently $v_l = 0, \forall l$), bearing in mind that $\lim_{v_l \rightarrow 0} Q(\tilde{\Phi}_{p,p,l}) = 1$ and $\lim_{v_l \rightarrow 0} Q(\tilde{\Phi}_{p,q,l}) = 0, p \neq q$, where $\tilde{\Phi}_{p,q,l} = (\omega_p - \omega_q - (\omega_c + \omega_q) v_l/c) T_s/2$. Setting $\tilde{\Psi}_{q,l,b} = \omega_q (\tau_l + \epsilon_{\text{clk}}) - \frac{\omega_c + \omega_q}{c} v_l b M T_s$, we compute the required derivatives as

$$\partial \mathbf{m}_b[p] / \partial \epsilon_{\text{clk}} = -j \sum_{q \in \mathcal{P}} \omega_q g[q] \sum_{l=0}^{L-1} h_l e^{-j \tilde{\Psi}_{q,l,b}} Q(\tilde{\Phi}_{p,q,l}) \mathbf{F}_R^H \mathbf{a}_{R,q}(\tilde{\theta}_{R,l}) \mathbf{a}_{T,q}^T(\tilde{\theta}_{T,l}) \mathbf{x}_b[q] \quad (64)$$

$$\partial \mathbf{m}_b[p] / \partial \tau_l = -j \sum_{q \in \mathcal{P}} \omega_q g[q] h_l e^{-j \tilde{\Psi}_{q,l,b}} Q(\tilde{\Phi}_{p,q,l}) \mathbf{F}_R^H \mathbf{a}_{R,q}(\tilde{\theta}_{R,l}) \mathbf{a}_{T,q}^T(\tilde{\theta}_{T,l}) \mathbf{x}_b[q], \quad (65)$$

$$\partial \mathbf{m}_b[p] / \partial \tilde{\theta}_{T,l} = \sum_{q \in \mathcal{P}} g[q] h_l e^{-j \tilde{\Psi}_{q,l,b}} Q(\tilde{\Phi}_{p,q,l}) \mathbf{F}_R^H \mathbf{a}_{R,q}(\tilde{\theta}_{R,l}) \mathbf{a}_{T,q}^T(\tilde{\theta}_{T,l}) \mathbf{D}_{T,q}^T(\tilde{\theta}_{T,l}) \mathbf{x}_b[q], \quad (66)$$

$$\partial \mathbf{m}_b[p] / \partial \tilde{\theta}_{R,l} = \sum_{q \in \mathcal{P}} g[q] h_l e^{-j \tilde{\Psi}_{q,l,b}} Q(\tilde{\Phi}_{p,q,l}) \mathbf{F}_R^H \mathbf{D}_{R,q}(\tilde{\theta}_{R,l}) \mathbf{a}_{R,q}(\tilde{\theta}_{R,l}) \mathbf{a}_{T,q}^T(\tilde{\theta}_{T,l}) \mathbf{x}_b[q], \quad (67)$$

$$\partial \mathbf{m}_b[p] / \partial h_{l,\Re} = \sum_{q \in \mathcal{P}} g[q] e^{-j \tilde{\Psi}_{q,l,b}} Q(\tilde{\Phi}_{p,q,l}) \mathbf{F}_R^H \mathbf{a}_{R,q}(\tilde{\theta}_{R,l}) \mathbf{a}_{T,q}^T(\tilde{\theta}_{T,l}) \mathbf{x}_b[q], \quad (68)$$

$$\partial \mathbf{m}_b[p] / \partial h_{l,\Im} = j \partial \mathbf{m}_b[p] / \partial h_{l,\Re}, \quad (69)$$

$$\partial \mathbf{m}_b[p] / \partial v_l = \sum_{q \in \mathcal{P}} g[q] h_l e^{-j \tilde{\Psi}_{q,l,b}} Q(\tilde{\Phi}_{p,q,l}) V_{b,p,q,l} \mathbf{F}_R^H \mathbf{a}_{R,q}(\tilde{\theta}_{R,l}) \mathbf{a}_{T,q}^T(\tilde{\theta}_{T,l}) \mathbf{x}_b[q], \quad (70)$$

where $\mathbf{D}_{T,q}(\tilde{\theta}_{T,l})$ is a diagonal matrix with $[\mathbf{D}_{T,q}(\tilde{\theta}_{T,l})]_{j,j} = -j \frac{\omega_c + \omega_q}{c} d_{T,j} \mathbf{u}_\perp^T(\tilde{\theta}_{T,l}) \mathbf{u}(\psi_{T,j})$ and $\mathbf{D}_{R,p}(\tilde{\theta}_{R,l})$ is defined accordingly. Also

$$V_{b,p,q,l} = (\cot(\tilde{\Phi}_{p,q,l}) - N \cot(N \tilde{\Phi}_{p,q,l})) T_s / 2 + j(bM + (N - 1)/2) T_s. \quad (71)$$

APPENDIX B

ENTRIES OF FISHER INFORMATION TRANSFORMATION MATRICES

The entries of \mathbf{T}_T (\mathbf{T}_R) corresponding to identical parameters in ϕ and $\tilde{\phi}_T$ ($\tilde{\phi}_R$) are equal to 1, e.g. $\partial \epsilon_{\text{clk}} / \partial \epsilon_{\text{clk}} = 1$. Setting $d_{T,R} = \|\mathbf{p}_R - \mathbf{p}_T\|_2$, $d_{T,s,l} = \|\mathbf{p}_{s,l} - \mathbf{p}_T\|_2$ and $d_{R,s,l} = \|\mathbf{p}_R - \mathbf{p}_{s,l}\|_2$, the rest non-zero entries are computed as follows:

$$\partial \tau_l / \partial \mathbf{p}_R = -\mathbf{u}(\theta_{R,l}) / c, \quad (72) \quad \partial \tau_l / \partial \mathbf{p}_T = -\mathbf{u}(\theta_{T,l}) / c, \quad (76)$$

$$\partial \tilde{\theta}_{T,l} / \partial \mathbf{p}_R = \begin{cases} \frac{\mathbf{u}_\perp(\theta_{R,l})}{d_{T,R}}, & l\text{-th path is LOS,} \\ \mathbf{0}, & \text{otherwise,} \end{cases} \quad (73) \quad \partial \tilde{\theta}_{T,l} / \partial \mathbf{p}_T = \begin{cases} \frac{\mathbf{u}_\perp(\theta_{T,l})}{d_{T,R}}, & l\text{-th path is LOS,} \\ \frac{\mathbf{u}_\perp(\theta_{T,l})}{d_{T,s,l}}, & \text{otherwise,} \end{cases} \quad (77)$$

$$\partial \tilde{\theta}_{R,l} / \partial \mathbf{p}_R = \begin{cases} \frac{\mathbf{u}_\perp(\theta_{R,l})}{d_{T,R}}, & l\text{-th path is LOS,} \\ \frac{\mathbf{u}_\perp(\theta_{R,l})}{d_{R,s,l}}, & \text{otherwise,} \end{cases} \quad (74) \quad \partial \tilde{\theta}_{R,l} / \partial \mathbf{p}_T = \begin{cases} \frac{\mathbf{u}_\perp(\theta_{T,l})}{d_{T,R}}, & l\text{-th path is LOS,} \\ \mathbf{0}, & \text{otherwise,} \end{cases} \quad (78)$$

$$\partial \tilde{\theta}_{R,l} / \partial \alpha_R = -1, \quad (75) \quad \partial \tilde{\theta}_{T,l} / \partial \alpha_T = -1, \quad (79)$$

$$\partial \tau_l / \partial \mathbf{p}_{s,l} = (\mathbf{u}(\theta_{T,l}) + \mathbf{u}(\theta_{R,l})) / c, \quad (80)$$

$$\partial \tilde{\theta}_{T,l} / \partial \mathbf{p}_{s,l} = -\mathbf{u}_\perp(\theta_{T,l}) / d_{T,s,l}, \quad (81)$$

$$\partial \tilde{\theta}_{R,l} / \partial \mathbf{p}_{s,l} = -\mathbf{u}_\perp(\theta_{R,l}) / d_{R,s,l}. \quad (82)$$

For a mobile receiver

$$\partial v_l / \partial \mathbf{p}_R = -\rho_l \mathbf{u}_\perp(\theta_{R,l}) \begin{cases} 1/d_{T,R}, & l\text{-th path is LOS,} \\ 1/d_{R,s,l}, & \text{otherwise,} \end{cases} \quad (83)$$

$$\partial v_l / \partial \mathbf{v}_R = \mathbf{u}(\theta_{R,l}), \quad (84)$$

$$\partial v_l / \partial \mathbf{p}_{s,l} = \rho_l \mathbf{u}_\perp(\theta_{R,l}) / d_{R,s,l}, \quad (85)$$

where $\rho_l = \mathbf{v}_R^T \mathbf{u}_\perp(\theta_{R,l})$. Similar expressions can be obtained for a mobile transmitter.

APPENDIX C

PROOF OF THEOREM 1

We first have to compute the asymptotic expressions for the entries of the channel parameters FIM \mathbf{J}_ϕ . In order to facilitate readability and understanding, instead of referring to the entries of $\mathbf{J}_\phi^{(0)}$ by their position in the matrix, e.g. $[\mathbf{J}_\phi^{(0)}]_{1,3}$, we refer to them by using as indices the variables they correspond to, e.g. $J_{\epsilon_{\text{clk}}\tilde{\theta}_{T,0}}$. Using (33), (36) and (64)-(69) and the assumptions 1-3 of Section V, we find that

$$J_{\epsilon_{\text{clk}}\epsilon_{\text{clk}}} \rightarrow \delta_{R,T} \sum_{p \in \mathcal{P}} \gamma_p \omega_p^2 \sum_{l=0}^{L-1} |h_l|^2, \quad (86) \quad J_{h_l, \mathfrak{R} h_l, \mathfrak{R}} = J_{h_l, \mathfrak{I} h_l, \mathfrak{I}} = \delta_{R,T}, \quad (90)$$

$$J_{\tau_l \tau_l} = J_{\epsilon_{\text{clk}} \tau_l} \rightarrow \delta_{R,T} \sum_{p \in \mathcal{P}} \gamma_p \omega_p^2 |h_l|^2, \quad (87) \quad J_{\epsilon_{\text{clk}} h_l, \mathfrak{R}} = J_{\tau_l h_l, \mathfrak{R}} \rightarrow \delta_{R,T} h_l, \mathfrak{I} \sum_{p \in \mathcal{P}} \gamma_p \omega_p, \quad (91)$$

$$J_{\tilde{\theta}_{T,l} \tilde{\theta}_{T,l}} = \delta_{R,T} |h_l|^2 (\bar{\omega}_c/c)^2 S_T(\tilde{\theta}_{T,l}), \quad (88) \quad J_{\epsilon_{\text{clk}} h_l, \mathfrak{I}} = J_{\tau_l h_l, \mathfrak{I}} \rightarrow -\delta_{R,T} h_l, \mathfrak{R} \sum_{p \in \mathcal{P}} \gamma_p \omega_p, \quad (92)$$

$$J_{\tilde{\theta}_{R,l} \tilde{\theta}_{R,l}} = \delta_{R,T} |h_l|^2 (\bar{\omega}_c/c)^2 S_R(\tilde{\theta}_{R,l}), \quad (89)$$

where with some abuse of notation the equality sign is used to denote that the asymptotic values are equal. Using the notion of the EFIM, we can show that as far as position and orientation information is concerned, we can exclude the channel gains from the parameter vectors, as long as we include the uncertainty they introduce to the model by replacing the time-related FIM entries $J_{\epsilon_{\text{clk}}\epsilon_{\text{clk}}}, \{J_{\tau_l \tau_l}, J_{\epsilon_{\text{clk}} \tau_l}\}_{l=0}^{L-1}$ with $J'_{\epsilon_{\text{clk}}\epsilon_{\text{clk}}}, \{J'_{\tau_l \tau_l}, J'_{\epsilon_{\text{clk}} \tau_l}\}_{l=0}^{L-1}$, where $J'_{\epsilon_{\text{clk}}\epsilon_{\text{clk}}} \rightarrow \delta_{R,T} \beta^2 \sum_{l=0}^{L-1} |h_l|^2$ and $J'_{\tau_l \tau_l} = J'_{\epsilon_{\text{clk}} \tau_l} \rightarrow \delta_{R,T} \beta^2 |h_l|^2$. Using the favorable propagation conditions (33)-(35) and following the Bachmann-Landau asymptotic notations⁴ [35], we can show that all the diagonal entries of the FIM and $J_{\epsilon_{\text{clk}} \tau_l}$ are $\Theta(x^3)$, where $x \in N_T, N_R, F_s$, e.g. $J_{\tau_l \tau_l} = \Theta(N_R F_s^2)$, and the rest of the entries are $o(x^3)$, which means they can be ignored in the computation of the asymptotic position and orientation EFIM. For brevity, we only present the derivation for the case when the LOS path is available. In order to make the expressions more compact, when the same variable is used in both indices we write it only once; e.g. we write $J'_{\epsilon_{\text{clk}}}$ instead of $J'_{\epsilon_{\text{clk}}\epsilon_{\text{clk}}}$.

⁴ $f(x) = o(g(x))$ means that $\lim_{x \rightarrow \infty} \left| \frac{f(x)}{g(x)} \right| = 0$ and $f(x) = \Theta(g(x))$ means that $0 < \liminf_{x \rightarrow \infty} \left| \frac{f(x)}{g(x)} \right| \leq \limsup_{x \rightarrow \infty} \left| \frac{f(x)}{g(x)} \right| < \infty$

Using the expressions from Appendix B for the entries of the Fisher information transformation matrices, we compute

$$\mathbf{T}_{\text{po}} \mathbf{J}_\phi \mathbf{T}_{\text{po}}^\top = \frac{J'_{\tau_0}}{c^2} \mathbf{z}_{\tau_0} \mathbf{z}_{\tau_0}^\top + \frac{J_{\tilde{\theta}_{\tau,0}}}{d_{\text{T,R}}^2} \mathbf{z}_{\theta_{\tau,0}} \mathbf{z}_{\theta_{\tau,0}}^\top + \frac{J_{\tilde{\theta}_{\text{R},0}}}{d_{\text{T,R}}^2} \mathbf{z}_{\theta_{\text{R},0}} \mathbf{z}_{\theta_{\text{R},0}}^\top + \sum_{l=1}^{L-1} \left(\frac{J'_{\tau_l}}{c^2} \mathbf{z}_{\tau_l} \mathbf{z}_{\tau_l}^\top + \frac{J_{\tilde{\theta}_{\text{R},l}}}{d_{\text{R},s,l}^2} \mathbf{z}_{\theta_{\text{R},l}} \mathbf{z}_{\theta_{\text{R},l}}^\top \right), \quad (93)$$

where $\mathbf{z}_{\tau_l} = [-\mathbf{u}^\top(\theta_{\text{R},l}), 0]^\top$ and $\mathbf{z}_{\theta_{\text{R},l}} = [\mathbf{u}_\perp^\top(\theta_{\text{R},l}), -d_{\text{R},s,l}]^\top$. We also write

$$\mathbf{T}_{\text{np}} \mathbf{J}_\phi \mathbf{T}_{\text{np}}^\top = \begin{bmatrix} J'_{\epsilon_{\text{clk}}} + \frac{1}{\sigma_{\text{clk}}^2} & \mathbf{b}^\top \\ \mathbf{b} & \mathbf{C} \end{bmatrix}, \quad (94)$$

where $\mathbf{b} = [J'_{\tau_1} \boldsymbol{\nu}_1^\top / c, \dots, J'_{\Delta\tau_{L-1}} \boldsymbol{\nu}_{L-1}^\top / c]^\top$, $\boldsymbol{\nu}_l = \mathbf{u}(\theta_{\text{T},l}) + \mathbf{u}(\theta_{\text{R},l})$ and \mathbf{C} is a block diagonal matrix with the following 2×2 matrices on its diagonal:

$$\mathbf{J}_{s,l} = \frac{J'_{\tau_l}}{c^2} \boldsymbol{\nu}_l \boldsymbol{\nu}_l^\top + \frac{J_{\tilde{\theta}_{\text{T},l}}}{d_{\text{T},s,l}^2} \mathbf{u}_\perp(\theta_{\text{T},l}) \mathbf{u}_\perp^\top(\theta_{\text{T},l}) + \frac{J_{\tilde{\theta}_{\text{R},l}}}{d_{\text{R},s,l}^2} \mathbf{u}_\perp(\theta_{\text{R},l}) \mathbf{u}_\perp^\top(\theta_{\text{R},l}). \quad (95)$$

In order to compute $(\mathbf{T}_{\text{np}} \mathbf{J}_\phi \mathbf{T}_{\text{np}}^\top)^{-1}$ using block matrix inversion, we still need to compute \mathbf{C}^{-1} , which in turn, using block diagonal matrix inversion, requires the computation of $\mathbf{J}_{s,l}^{-1}$. We compute $\mathbf{J}_{s,l}^{-1}$ as [12, Lemma 1]

$$\mathbf{J}_{s,l}^{-1} = \frac{1}{|\mathbf{J}_{s,l}|} \left[\frac{J'_{\tau_l}}{c^2} \boldsymbol{\nu}_{l,\perp} \boldsymbol{\nu}_{l,\perp}^\top + \frac{J_{\tilde{\theta}_{\text{T},l}}}{d_{\text{T},s,l}^2} \mathbf{u}(\theta_{\text{T},l}) \mathbf{u}^\top(\theta_{\text{T},l}) + \frac{J_{\tilde{\theta}_{\text{R},l}}}{d_{\text{R},s,l}^2} \mathbf{u}(\theta_{\text{R},l}) \mathbf{u}^\top(\theta_{\text{R},l}) \right], \quad (96)$$

with $\boldsymbol{\nu}_{l,\perp} = \mathbf{u}_\perp(\theta_{\text{T},l}) + \mathbf{u}_\perp(\theta_{\text{R},l})$ and

$$|\mathbf{J}_{s,l}| = \frac{J'_{\tau_l}}{c^2} (1 + \cos(\Delta\theta_l))^2 \left(\frac{J_{\tilde{\theta}_{\text{T},l}}}{d_{\text{T},s,l}^2} + \frac{J_{\tilde{\theta}_{\text{R},l}}}{d_{\text{R},s,l}^2} \right) + \frac{J_{\tilde{\theta}_{\text{T},l}} J_{\tilde{\theta}_{\text{R},l}}}{d_{\text{T},s,l}^2 d_{\text{R},s,l}^2} \sin^2(\Delta\theta_l). \quad (97)$$

Therefore, using (94)-(97), $\mathbf{u}^\top(\theta_{\text{T},l}) \mathbf{u}(\theta_{\text{R},l}) = \cos(\Delta\theta_l)$ and $\mathbf{u}^\top(\theta_{\text{T},l}) \mathbf{u}_\perp(\theta_{\text{R},l}) = \sin(\Delta\theta_l)$, after some algebraic manipulations we find that

$$\begin{aligned} \mathbf{T}_{\text{po}} \mathbf{J}_\phi \mathbf{T}_{\text{np}}^\top (\mathbf{T}_{\text{np}} \mathbf{J}_\phi \mathbf{T}_{\text{np}}^\top)^{-1} \mathbf{T}_{\text{np}} \mathbf{J}_\phi \mathbf{T}_{\text{po}}^\top &= \sum_{l=1}^{L-1} \left[\frac{(J'_{\tau_l})^2 (1 + \cos(\Delta\theta_l))^2}{c^4 |\mathbf{J}_{s,l}|} \left(\frac{J_{\tilde{\theta}_{\text{T},l}}}{d_{\text{T},s,l}^2} + \frac{J_{\tilde{\theta}_{\text{R},l}}}{d_{\text{R},s,l}^2} \right) \mathbf{z}_{\tau_l} \mathbf{z}_{\tau_l}^\top \right. \\ &+ \frac{J_{\tilde{\theta}_{\text{R},l}}^2}{d_{\text{R},s,l}^4} \left(\frac{J'_{\tau_l} (1 + \cos(\Delta\theta_l))^2}{c^2 |\mathbf{J}_{s,l}|} + \frac{J_{\tilde{\theta}_{\text{T},l}} \sin^2(\Delta\theta_l)}{d_{\text{T},s,l}^2 |\mathbf{J}_{s,l}|} \right) \mathbf{z}_{\theta_{\text{R},l}} \mathbf{z}_{\theta_{\text{R},l}}^\top \\ &\left. + \frac{J'_{\tau_l} J_{\tilde{\theta}_{\text{T},l}} J_{\tilde{\theta}_{\text{R},l}} (1 + \cos(\Delta\theta_l)) \sin(\Delta\theta_l)}{c^2 d_{\text{T},s,l}^2 d_{\text{R},s,l}^2 |\mathbf{J}_{s,l}|} \left(\mathbf{z}_{\tau_l} \mathbf{z}_{\theta_{\text{R},l}}^\top + \mathbf{z}_{\theta_{\text{R},l}} \mathbf{z}_{\tau_l}^\top \right) \right] + \frac{1}{\hat{K}_{\epsilon_{\text{clk}}}} \hat{\mathbf{z}}_{\epsilon_{\text{clk}}} \hat{\mathbf{z}}_{\epsilon_{\text{clk}}}^\top, \quad (98) \end{aligned}$$

where

$$\begin{aligned} \hat{K}_{\epsilon_{\text{clk}}} &= \frac{J'_{\epsilon_{\text{clk}}} + \frac{1}{\sigma_{\text{clk}}^2} - \sum_{l=1}^{L-1} J'_{\tau_l}}{c^2} + \sum_{l=1}^{L-1} \left[\frac{J'_{\tau_l} J_{\tilde{\theta}_{\text{T},l}} J_{\tilde{\theta}_{\text{R},l}}}{c^2 d_{\text{T},s,l}^2 d_{\text{R},s,l}^2 |\mathbf{J}_{s,l}|} \sin^2(\Delta\theta_l) \right], \\ \hat{\mathbf{z}}_{\epsilon_{\text{clk}}} &= \sum_{l=1}^{L-1} \frac{J'_{\tau_l} J_{\tilde{\theta}_{\text{T},l}} J_{\tilde{\theta}_{\text{R},l}}}{c^2 d_{\text{T},s,l}^2 d_{\text{R},s,l}^2 |\mathbf{J}_{s,l}|} \sin(\Delta\theta_l) \mathbf{z}_l. \end{aligned}$$

Combining (93) and (98) we obtain the desired result.

REFERENCES

- [1] A. Dammann, R. Raulefs, and S. Zhang, "On prospects of positioning in 5G," in *IEEE Int. Conf. Commun. Workshop (ICCW)*, London, UK, Jun. 2015, pp. 1207–1213.
- [2] K. Witrisal *et al.*, "High-accuracy localization for assisted living: 5G systems will turn multipath channels from foe to friend," *IEEE Signal Process. Mag.*, vol. 33, no. 2, pp. 59–70, Mar. 2016.
- [3] K. Witrisal, S. Hinteregger, J. Kulmer, E. Leitinger, and P. Meissner, "High-accuracy positioning for indoor applications: RFID, UWB, 5G, and beyond," in *IEEE 10th Int. Conf. RFID (RFID)*, Orlando, FL, USA, May 2016, pp. 1–7.
- [4] H. Wymeersch, G. Seco-Granados, G. Destino, D. Dardari, and F. Tufvesson, "5G mmWave positioning for vehicular networks," *IEEE Wireless Commun.*, vol. 24, no. 6, pp. 80–86, Dec. 2017.
- [5] A. Kakkavas, M. H. Castañeda Garcia, R. A. Stirling-Gallacher, and J. A. Nossek, "Multi-array 5G V2V relative positioning: Performance bounds," in *IEEE Global Commun. Conf. (GLOBECOM)*, Abu Dhabi, UAE, Dec. 2018, pp. 206–212.
- [6] A. Hakkarainen, J. Werner, M. Costa, K. Leppanen, and M. Valkama, "High-efficiency device localization in 5G ultra-dense networks: Prospects and enabling technologies," in *IEEE 82th Veh. Technol. Conf. (VTC-Fall)*, Boston, MA, USA, Sep. 2015, pp. 1–5.
- [7] P. Kela *et al.*, "Location based beamforming in 5G ultra-dense networks," in *IEEE 84th Vehicular Technology Conference (VTC-Fall)*, Montréal, Canada, Sep. 2016, pp. 1–7.
- [8] F. Maschietti, D. Gesbert, P. de Kerret, and H. Wymeersch, "Robust location-aided beam alignment in millimeter wave massive MIMO," in *IEEE Global Commun. Conf. (GLOBECOM)*, Singapore, Dec. 2017, pp. 1–6.
- [9] Y. Shen and M. Z. Win, "Fundamental limits of wideband localization - part I: A general framework," *IEEE Trans. Inf. Theory*, vol. 56, no. 10, pp. 4956–4980, Oct. 2010.
- [10] Y. Shen, H. Wymeersch, and M. Z. Win, "Fundamental limits of wideband localization - part II: Cooperative networks," *IEEE Trans. Inf. Theory*, vol. 56, no. 10, pp. 4981–5000, Oct. 2010.
- [11] Y. Shen and M. Z. Win, "Fundamental limits of wideband localization accuracy via Fisher information," in *IEEE Wireless Commun. Netw. Conf. (WCNC)*, Kowloon, Hong Kong, Mar. 2007, pp. 3046–3051.
- [12] —, "On the use of multipath geometry for wideband cooperative localization," in *IEEE Global Commun. Conf. (GLOBECOM)*, Honolulu, HI, USA, Nov. 2009, pp. 1–6.
- [13] Y. Han, Y. Shen, X. P. Zhang, M. Z. Win, and H. Meng, "Performance limits and geometric properties of array localization," *IEEE Trans. Inf. Theory*, vol. 62, no. 2, pp. 1054–1075, Feb. 2016.
- [14] A. Guerra, F. Guidi, and D. Dardari, "Position and orientation error bound for wideband massive antenna arrays," in *IEEE Int. Conf. Commun. Workshop (ICCW)*, London, UK, Jun. 2015, pp. 853–858.
- [15] —, "Single anchor localization and orientation performance limits using massive arrays: MIMO vs. beamforming," *IEEE Trans. Wireless Commun.*, vol. 17, no. 8, pp. 5241–5255, Aug. 2018.
- [16] A. Shahmansoori, G. E. Garcia, G. Destino, G. Seco-Granados, and H. Wymeersch, "5G position and orientation estimation through millimeter wave MIMO," in *IEEE Globecom Workshops (GC Wkshps)*, San Diego, CA, USA, Dec. 2015, pp. 1–6.
- [17] Z. Abu-Shaban, X. Zhou, T. D. Abhayapala, G. Seco-Granados, and H. Wymeersch, "Error bounds for uplink and downlink 3D localization in 5G mmWave systems," *IEEE Trans. Wireless Commun.*, vol. 17, no. 8, pp. 4939–4954, Aug. 2018.
- [18] R. Mendrzik, H. Wymeersch, G. Bauch, and Z. Abu-Shaban, "Harnessing NLOS components for position and orientation estimation in 5G millimeter wave MIMO," *IEEE Trans. Wireless Commun.*, vol. 18, no. 1, pp. 93–107, Jan. 2019.
- [19] A. Shahmansoori, G. E. Garcia, G. Destino, G. Seco-Granados, and H. Wymeersch, "Position and orientation estimation through millimeter-wave MIMO in 5G systems," *IEEE Trans. Wireless Commun.*, vol. 17, no. 3, pp. 1822–1835, Mar. 2018.

- [20] Y. Wang, Y. Wu, and Y. Shen, "Joint spatiotemporal multipath mitigation in large-scale array localization," *IEEE Trans. Signal Process.*, vol. 67, no. 3, pp. 783–797, Feb. 2019.
- [21] J. Talvitie, M. Valkama, G. Destino, and H. Wymeersch, "Novel algorithms for high-accuracy joint position and orientation estimation in 5G mmWave systems," in *IEEE Globecom Workshops (GC Wkshps)*, Singapore, Dec. 2017, pp. 1–7.
- [22] R. Mendrzik, H. Wymeersch, and G. Bauch, "Joint localization and mapping through millimeter wave MIMO in 5G systems," in *IEEE Global Commun. Conf. (GLOBECOM)*, Abu Dhabi, UAE, Dec. 2018, pp. 1–6.
- [23] Z. Abu-Shaban, H. Wymeersch, T. D. Abhayapala, and G. Seco-Granados, "Single-anchor two-way localization bounds for 5G mmWave systems: Two protocols," *CoRR*, vol. abs/1805.02319, 2018. [Online]. Available: <http://arxiv.org/abs/1805.02319>
- [24] Y. Liu, Y. Shen, and M. Z. Win, "Single-anchor localization and synchronization of full-duplex agents," *IEEE Trans. Commun.*, pp. 1–1, Oct. 2018.
- [25] R. Vaughan and J. Bach-Anderson, *Channels, propagation and antennas for mobile communications*, ser. IEE electromagnetic waves series. Stevenage: The Institution of Engineering and Technology, 2003.
- [26] T. S. Rappaport, E. Ben-Dor, J. N. Murdock, and Y. Qiao, "38 Ghz and 60 Ghz angle-dependent propagation for cellular & peer-to-peer wireless communications," in *IEEE Int. Conf. Commun. (ICC)*, Ottawa, Canada, Jun. 2012, pp. 4568–4573.
- [27] M. T. Martinez-Ingles, D. P. Gaillot, J. Pascual-Garcia, J. M. Molina-Garcia-Pardo, M. Lienard, and J. V. Rodríguez, "Deterministic and experimental indoor mmW channel modeling," *IEEE Antennas Wireless Propag. Lett.*, vol. 13, pp. 1047–1050, 2014.
- [28] M. Peter *et al.*, "Measurement campaigns and initial channel models for preferred suitable frequency ranges; Deliverable D2.1," Mar. 2016. [Online]. Available: <https://5g-mmmagic.eu/results/#deliverables>
- [29] T. Rappaport, *Wireless Communications: Principles and Practice*, 2nd ed. Upper Saddle River, NJ, USA: Prentice Hall PTR, 2001.
- [30] H. L. Van Trees and K. L. Bell, *Detection, Estimation and Modulation Theory, Part I: Detection, Estimation, and Filtering Theory*, 2nd ed. John Wiley & Sons, 2013.
- [31] E. L. Lehmann and G. Casella, *Theory of Point Estimation*, 2nd ed. Springer New York, Aug. 1998.
- [32] J. Chen, "When does asymptotic orthogonality exist for very large arrays?" in *IEEE Global Commun. Conf. (GLOBECOM)*, Atlanta, GA, USA, Dec. 2013, pp. 4146–4150.
- [33] H. Q. Ngo, E. G. Larsson, and T. L. Marzetta, "Aspects of favorable propagation in massive MIMO," in *22nd European Signal Processing Conference (EUSIPCO)*, Lisbon, Portugal, Sep. 2014, pp. 76–80.
- [34] C. Masouros and M. Matthaiou, "Space-constrained massive MIMO: Hitting the wall of favorable propagation," *IEEE Commun. Lett.*, vol. 19, no. 5, pp. 771–774, May 2015.
- [35] T. H. Cormen, C. E. Leiserson, R. L. Rivest, and C. Stein, *Introduction to Algorithms, Third Edition*, 3rd ed. The MIT Press, 2009.